

In This Issue:

Departments

News Briefs and Reports

DEVELOPMENTS

347

NBS Awards Two 1988 Precision Measurement Grants
NBS Seeks Project Proposals for 1989 Precision Measurement Grants
Six NBS Projects Win 1987 I-R 100 Awards
New Superconductor Applications Closer with Electrical Contacts Discovery
NBS Contributes to Thin-Film Superconductor Research
NBS Setting Up "Next Generation" ISDN Laboratory
Prototype IRDS Software Being Evaluated
Bureau Researcher Designs Novel Humidity Sensing Device
"Expert System" May Boost Semiconductor Productivity
NBS/Aluminum Industry Develop Temperature Sensor
Industry and NBS Join in Advanced Ceramics Effort
New Federal Standard for BASIC Is Approved

STANDARD REFERENCE DATA

352

NBS/EPA/MSDC Mass Spectral Database Available for PC Users

STANDARD REFERENCE MATERIALS

353

AST Enzyme Levels Can Be Checked with New Materials

NBS SERVICES

353

NBS Electromagnetics Laboratory Accreditation Program Expanded to Meet
Industrial and Defense Needs

Conferences/Events

International Standards for Nondestructive Testing A Report on the Sixth Plenary Meeting of ISO TC 135, Yokohama, Japan, May 11–15, 1987	Leonard Mordfin	387
Superconductivity: Challenge for the Future Federal Conference on Commercial Applications of Superconductivity, Washington, DC, July 28–29, 1987	Robert A. Kamper and Alan F. Clark	391

CALENDAR

393

SUBJECT AND AUTHOR INDEX TO VOLUME 92

395

Articles

Transient Impact Response of Thick Circular Plates	Mary Sansalone and Nicholas J. Carino	355
Transient Impact Response of Plates Containing Flaws	Mary Sansalone and Nicholas J. Carino	369
A Low Noise Cascode Amplifier	Steven R. Jefferts and F. L. Walls	383

News Briefs and Reports

Developments

NBS AWARDS TWO 1988 PRECISION MEASUREMENT GRANTS

NBS has awarded two new Precision Measurement Grants for studies of atomic energy levels in multi-electron atoms, and the quantized Hall effect.

The awards, for \$30,000 each for fiscal year 1988, went to Professor John D. Morgan, III of the University of Delaware, for theoretical work on the calculation of helium atom energy levels, and to Professor Wiley P. Kirk of Texas A&M University, for work on the sources of error in measuring the quantized Hall resistance.

Morgan's project deals with theoretical calculations of helium atom energy levels. The helium atom is something of a guinea pig for atomic physics: complex enough to be interesting, simple enough to be manageable. Since the 1920s theoreticians and experimentalists have studied the helium atom to see how accurately energy values calculated from quantum electrodynamics (QED) theory correspond with measured values. This serves as a test for fundamental principles of quantum theory.

In recent years, experimental physicists armed with sophisticated techniques in laser spectroscopy have outstripped their theoretician colleagues, making energy-level measurements at accuracies better than 10^{-4} cm⁻¹. This is approximately 10 times better than the best theoretical calculations, which are hampered by the fiendish complexity of interactions in quantum theory.

Morgan's proposal is to push theoretical calculations of ground and excited states of the helium atom at least far enough to match the accuracy of current experimental work. This requires making allowance for several effects that were insignificant

at lesser accuracies. The combination of Morgan's results with experimental results (supported by previous Precision Measurement Grants) will provide a stringent test of some fundamental aspects of QED theory.

Kirk's work relates directly to design of fundamental standards of electrical resistance. The quantized Hall effect, the discovery of which won German physicist Klaus von Klitzing the 1985 Nobel prize in physics, says that the electrical resistance across the width of a semiconductor strip under special conditions, including low temperature and high magnetic field, goes up in steps or "plateaus" which are simply integer multiples of a combination of basic constants of nature. Standards laboratories around the world leaped on this discovery as the potential basis for new electrical resistance standards based directly on natural constants.

Kirk proposes a series of experiments on three known problems that contribute to error in measuring the quantized Hall resistance to determine in what measure they affect the accuracy of resistance standards and closely related efforts to measure the value of the physical quantity known as the fine-structure constant. One of the fundamental parameters of quantum electrodynamics, the fine-structure constant relates to electrical and magnetic interactions of subatomic particles.

Kirk's work should also provide valuable insight into the structure of the Hall plateaus.

The Precision Measurement Grants Program is administered by Barry N. Taylor, B258 Metrology Building, National Bureau of Standards, Gaithersburg, MD 20899.

NBS SEEKS PROJECT PROPOSALS FOR 1989 PRECISION MEASUREMENT GRANTS

NBS is seeking project proposals for two research grants for fiscal year 1989 in the field of precision measurement and fundamental constants.

The Precision Measurement Grants are for \$30,000 for one year, and may be renewed by NBS for up to two additional years. Prospective candidates must submit summaries of their proposed projects and biographical information to NBS by February 1, 1988, to be considered for the current grants, which will run from October 1988 through September 1989.

NBS Precision Measurement Grants are awarded each year to scientists in academic institutions for work in testing basic theories; determining values for fundamental constants; investigating related physical phenomena; or developing new, fundamental measurement methods.

The grants were instituted in 1970 to augment NBS research programs in physical constants and fundamental measurements, and to encourage research in these fields at U.S. colleges and universities. To date, 42 grants have been awarded in such areas as precision spectroscopy, the determination of mass ratios between atomic particles, a test of local Lorentz invariance, the precise timing of millisecond pulsars, and the redetermination of various constants, such as the gas constant and Rydberg constant.

Proposals are evaluated according to the importance of the proposed research; the relation of the project to the improvement of basic measurement units, physical standards, or measurement methodologies; the feasibility of the research; and past accomplishments of the applicant.

By February 1, applicants should submit a pre-proposal summary of not more than five double-spaced pages outlining the objective, motivation, and technical approach of the research, and the amount and source of current funding for the research, together with a concise biographical sketch of the applicant and a list of the applicant's most important publications. At least three copies of this material should be sent to Barry N. Taylor, chairman of the NBS Precision Measurement Grants Committee, B258 Metrology Building, National Bureau of Standards, Gaithersburg, MD 20899.

Four to eight candidates will be chosen by March 15 on the basis of this material and will be asked to submit more complete proposals. The final selection will be made by August 15, 1988.

For further information, contact Barry N. Taylor at the above address or call 301/975-4220.

SIX NBS PROJECTS WIN 1987 I-R 100 AWARDS

Innovations in semiconductors, sensors and measurement techniques for quality control, and chemistry were among the six projects from NBS to be given I-R 100 awards this year.

I-R 100 awards are given annually by *Research & Development* magazine to honor the "100 most significant" new technical products of the preceding year. Presentations were made in September in Chicago, bringing to 57 the number of I-R 100 awards NBS has received since first entering the competition in 1973.

Descriptions of the award-winning projects follow.

Crystal Axis Detection

Sidney Weiser of NBS (now retired) earned an I-R 100 award for the invention of an automated laser scanner that determines the orientation of the crystal axis in single-crystal semiconductor materials.

The proper alignment of crystal axes is an important element in the manufacture of semiconductor devices, which are fabricated on thin "wafers" sliced from a single crystal of silicon or other material. Weiser's crystal axis laser scanner was developed for a particularly difficult case: the crystals of cadmium telluride which are the heart of mercuric telluride infrared detectors.

Previous methods of determining the major axis of cadmium telluride crystals required the use of x-ray diffraction techniques, which work only on wafers and require from 5 to 20 minutes per observation. A more recent technique depends on the reflection of laser light from the crystal surface which has been selectively etched to highlight the crystal planes. Very low signal-to-noise ratios make this technique difficult to use.

Weiser's instrument uses a significant modification of the laser scattering approach and a computerized pattern recognition algorithm to make the same measurement in less than a second—so fast that the machine can easily prepare maps of multi-crystalline areas. The instrument works with both single wafers and the original crystal boule from which the wafers are cut.

Weiser's device will be manufactured commercially.

Surface Roughness Measurement

Four NBS researchers shared an I-R 100 award for their development of an automated technique using thermography to measure the roughness of surfaces and find defects. The procedure is faster and more versatile than current methods.

Being able to measure surface profiles and detect defects is important for quality control in industries such as electronics, automotive, ceramics, and construction. The NBS technique should be adaptable to in-line inspection since the measurements are

made quickly, without touching the surface, and the instrumentation requires little calibration.

In the NBS method, the material to be inspected is heated slightly and the resulting emissions are detected by an infrared thermographic camera. Using a microcomputer-based image processor, the thermographic image can be converted to an equivalent topographic map of the surface. Accompanying software mathematically describes surface roughness and isolates defects.

The technique was developed initially to measure very rough surfaces, such as steel which has been blasted with an abrasive like sand. But the NBS researchers are confident it also can measure the roughness of much finer surfaces. In addition, they have used it to find defects, such as rust spots under paint on metal surfaces.

Mary E. McKnight, Jonathan W. Martin, and Edward J. Embree of NBS and Dale P. Bentz, formerly of NBS and now with the W. R. Grace Corporation, developed the technique.

In-Situ Ceramic Quality Sensor

Martin P. Jones, formerly of NBS, and Gerald W. Blessing of NBS have won an I-R 100 award for the development of a new ultrasonic method for monitoring the quality of ceramic powders during compaction. The sensor is the first nondestructive evaluation technique that permits ceramic producers to fully automate the inspection of compacted powders while the material is in the mold. The sensor system uses piezoelectric transducers to generate ultrasonic wave pulses that travel through a mold and into a sample. The resulting ultrasonic echoes are recorded as they reflect back and forth through the material until the pulses die out. The sensor, which is sensitive to porosity, moisture, and chemical content, offers producers a way to control the quality of ceramic powders at almost any stage of compaction without having to handle the very fragile materials in their green or unfired state.

The in-situ ceramic quality sensor was developed at NBS as part of the Bureau's effort to apply nondestructive evaluation techniques to measure the properties and characteristics of materials for in-line monitoring and process control during manufacture. Jones, who now works for Alcoa Laboratories, Alcoa Center, PA, developed the sensor with Blessing while he was a Johns Hopkins University graduate student at NBS.

Ultrasound Pipe Porosity Sensor

An industry/government team was given an I-R 100 award for the development of another ultra-

sonic sensor technique that will enable steel producers to quickly detect flaws in hot metal and more accurately crop unsound material before it is run through the complete production cycle.

The sensor, which has the potential for saving the U.S. steel industry \$50 million annually, was developed under a cooperative agreement between NBS and the American Iron and Steel Institute (AISI) and evaluated and tested at Argonne National Laboratory. It is based on an ultrasonic system developed for AISI by the Magnaflux Corporation of Chicago.

The Magnaflux system uses contact rollers that require heavy pressures (10,000–20,000 pounds per square inch) to transmit high-frequency sound waves into hot steel.

Melvin Linzer of NBS modified this system by placing a powder flux—which melts at high temperatures—in front of the rollers. This eliminates the need for heavy wheel pressures to couple ultrasound pulses into and out of hot steel blooms, billets, and slabs. The award-winning technique uses a piezoelectric transducer that is isolated from the hot steel surface by a buffer rod. The powder flux is used as a liquid couplant to provide excellent acoustic contact between the rod and the hot steel surface.

The other members of the research team include Haydn N. G. Wadley, NBS; Lev Spevak, Magnaflux Corporation; David S. Kupperman, Argonne National Laboratory; and C. David Rogers, United States Steel, USX Corporation, and AISI program manager at NBS.

Digital Compositional Mapping

A team of eight researchers from NBS and the National Institutes of Health (NIH) has been honored for the introduction of a system that uses digital computer technology coupled with electron beam instruments to “map” the distribution of chemical elements on the surfaces of a variety of samples.

The key advantage to the system is that it can create compositional images which display both the type and number of atoms at sample sites 1 micrometer or finer in dimension. That is, besides giving qualitative information on which elements are distributed in the sample, the system also provides a complete quantitative analysis at every one-micrometer-wide point. The researchers can view these dual functions through a color-enhanced video image of the sample. Other devices on the market are limited in their ability to provide a complete quantitative analysis.

The system has many applications, including characterization of microstructures in various

materials and the linking of disease to chemical imbalances in the body.

The digital compositional mapping system was developed by Ryna B. Marinenko, Dale E. Newbury, Robert C. Myklebust, and David S. Bright, of NBS, and Charles E. Fiori, Richard D. Leapman, Carol R. Swyt, and Keith E. Gorlen of NIH.

Microwave Dissolution System

H. M. Kingston of NBS and Lois B. Jassie, Michael J. Collins, and Ronald J. Goetchius of CEM Corporation, a North Carolina manufacturer of research microwave equipment, are sharing an I-R 100 award for their design of a system that uses microwaves to rapidly dissolve chemical samples in closed vessels. Sample dissolution is the first step in most instrumental elemental analysis.

The new system is an improvement over traditional dissolution techniques. It is rapid, safe, and contaminant-free, factors essential to reliable chemical analyses. By combining the microwave technique's ability to directly couple energy and heat materials quickly with the superior dissolving properties of closed containers under pressure, the NBS/CEM team has designed a method for decomposing samples that takes less than 15 minutes. Older hot plate methods using open-vented beakers typically require dissolving times of anywhere from 4 hours to 4 days, depending on the complexity of the sample.

Kingston and Jassie are editing a book for the American Chemical Society that will allow industrial chemists to predict conditions and safely tailor their own microwave devices for desired results. Also, they have given microwave dissolution information and advice to more than 400 researchers from companies, universities, and research laboratories.

NEW SUPERCONDUCTOR APPLICATIONS CLOSER WITH ELECTRICAL CONTACTS DISCOVERY

NBS, in collaboration with the Westinghouse Research and Development Center, has devised a new method for making improved, lower-resistance electrical contacts on the new high-critical-temperature ceramic superconductors.

High contact resistance has been a major obstacle to commercial applications of the new superconductors. The new method reduces the contact resistivity several thousand times below that previously achieved with conventional contacts.

Resistance at electrical contacts causes heating in any device, but it is particularly fatal in superconductors. Even modest heating can raise the

temperature of the superconductor enough to weaken or destroy the property of superconductivity. In addition, for computer applications, heat generation is one of the primary factors limiting the number of circuit elements in a given volume and consequently, the ultimate speed of a computer. In magnet applications, there is the additional problem of needing large contact areas in order to handle very high currents. The new contact method is not restricted to small contact areas. The contacts made thus far have been about 10 square millimeters in size, but there is no inherent limitation preventing much larger contacts.

The new contact method developed by Jack W. Ekin of NBS and Armand J. Panson of Westinghouse, has achieved contact surface resistivities of less than 10 micro-ohm-cm², using bulk samples of the new yttrium-barium-copper-oxide ceramic superconductor (YBa₂Cu₃O₇), a typical high-temperature superconductor. This level of performance for the "super contacts" was achieved while operating the superconductor at the relatively high temperature of liquid nitrogen—77 K. Even lower contact resistances are expected when the technique is refined and with superconducting films, which are less granular.

The method for producing the contacts is carried out at room temperature. It should be directly applicable to making connections to thin films for computer applications as well as bulk samples for fabricating magnets such as those used in motors and generators.

A number of contacts have been made using the new method, and they have been found to be consistently reproducible. Stability of the contacts over time and with use appears to be excellent. Systematic tests conducted on contacts exposed to dry air over a 3-month period showed consistently low resistivity and little degradation with repeated cooling to 77 K and warming to room temperature.

For further information, contact Jack Ekin at the National Bureau of Standards, Boulder, CO 80303.

NBS CONTRIBUTES TO THIN-FILM SUPERCONDUCTOR RESEARCH

In a joint effort with The Johns Hopkins University Applied Physics Laboratory (APL), NBS prepared and characterized bulk target materials for a new laser-ablation technique, developed at APL, to deposit superconducting oxide thin films on substrates. The superconducting transition temperatures for ablated thin films of barium, yttrium, copper, and oxygen—the BYCO-1,2,3, compound—at 94.5 K, and for films of lanthanum,

strontium, copper, and oxygen at 41.5 K are the same as those measured for the bulk material used for ablation. The thin-film deposits were produced on unheated substrates, and no further processing was required. While the test samples were made on fused silica substrates, the new low-temperature method permits the preparation of high-critical-temperature superconducting materials on other substrates such as gallium arsenide that cannot withstand elevated temperatures during processing. The hybrid superconducting/semiconducting systems offer potential for smaller and faster integrated circuits.

For information on the superconducting thin-film program, contact Kishin Moorjani, The Johns Hopkins University Applied Physics Laboratory, Laurel, MD 20707, or call 301/953-6232. For information on the ceramic oxide materials, contact Lawrence H. Bennett, B150 Materials Building, National Bureau of Standards, Gaithersburg, MD 20899, or call 301/975-5966.

NBS SETTING UP "NEXT GENERATION" ISDN LABORATORY

The Integrated Services Digital Network (ISDN) is a new telecommunications technology that makes it possible to send and receive voice, data, and image signals simultaneously over existing telephone lines. To help the Federal Government make a smooth transition to ISDN, which is sometimes called the "next generation" of telecommunications technology, NBS is establishing an ISDN laboratory. It will be used primarily to demonstrate ISDN technology and develop standards and test methods. NBS is working with private industry, research laboratories, and other agencies of the Federal government to set up the ISDN laboratory using donated equipment and services.

For further information, contact Michael Wong, A216 Technology Building, National Bureau of Standards, Gaithersburg, MD 20899, or call 301/975-2942.

PROTOTYPE IRDS SOFTWARE BEING EVALUATED

More than 40 users from private industry and government, both in the United States and abroad, have agreed to use and evaluate prototype software developed by NBS. The software implements a draft industry standard for the Information Resource Dictionary System (IRDS).

The IRDS is a key computer software tool which can be used to record, store, and process information about an organization's data and data processing resources. NBS and the American

National Standards Institute have been working together for several years on the standard's technical specifications. But until now, software has not been available. IRDS standards for both industry and the Federal government are expected to be issued next year.

For more information on the IRDS software evaluation program, contact Alan Goldfine, A265 Technology Building, National Bureau of Standards, Gaithersburg, MD 20899, or call 301/975-3252.

BUREAU RESEARCHER DESIGNS NOVEL HUMIDITY SENSING DEVICE

An NBS scientist has received a patent for the design of a device that uses organic polymers to sense and measure humidity. Peter H. Huang has been granted patent number 4,681,855 for the invention, which is an improvement over existing devices because of its expected long life, lasting accuracy, and ability to be used at high temperatures and humidities. Huang envisions many potential applications, especially in controlling the drying processes that support industries such as textiles, paper, chemicals, and food. Meteorological and electronics applications also are feasible. Huang's system uses a halogen-based organic polymer such as Teflon onto which he deposits a mixture of a strong and a weak acid. By using this combination, he is able to "tune" the system to measure humidity over a wide range by varying the ratio of these acids. Because the water content of the polymer is directly related to relative humidity, the polymer can be measured electrically or weighed to determine its water content and, thus, the humidity. This approach significantly reduces hysteresis and increases sensitivity.

For further information, contact Peter Huang, B312 Physics Building, National Bureau of Standards, Gaithersburg, MD 20899, or call 301/975-2621.

"EXPERT SYSTEM" MAY BOOST SEMI-CONDUCTOR PRODUCTIVITY

An improved diagnostic tool that would help manufacturers pinpoint problems that could cause failures at various stages in the semiconductor wafer fabrication process is being developed jointly by NBS and the Westinghouse Research and Development Center. This still-experimental "expert system" offers diagnoses by imitating, through a computer, the collective intelligence and experience of fabrication experts.

The key advantage of the new system is that semiconductor process personnel who have com-

puter-stored data from test probes of wafers can use this data to diagnose fabrication problems on a personal computer screen in a readily understood, English-language format. Specialists with considerable expertise typically are needed in the semiconductor production process to interpret diagnostic test data, but such experts often are not available. The NBS/Westinghouse system is designed to substitute for specialists by supplying a human-like appraisal of critical test data.

Though the system is still in its formative stages, companies interested in working collaboratively with NBS may contact Loren W. Linholm, B360 Technology Building, National Bureau of Standards, Gaithersburg, MD 20899, or call 301/975-2052.

NBS/ALUMINUM INDUSTRY DEVELOP TEMPERATURE SENSOR

A process control sensor that rapidly measures the internal temperatures of extruded aluminum as it comes out of a die has been developed by NBS and the Extruded Products Division of the Aluminum Association. The new sensor can measure the body temperatures of extruded aluminum at 500 °C to a depth of one-half the thickness of the material, and with an accuracy of 5 °C.

Based on an electromagnetic concept, the sensor generates eddy currents in hot aluminum as it is extruded from a die. By measuring the properties of eddy currents in metal, it is possible to determine temperature. Electromagnetic signals from the extruded material are recorded by a computer and rapidly processed to show temperature for on-line process control.

The automated system also is designed to measure the dimensions of extruded materials as they come out of the press. This capability could be used to provide information on die wear and for other dimensional sensor needs such as in hot isostatic pressing. The sensor was designed by Michael L. Mester, an Aluminum Association-sponsored researcher at NBS, and by NBS scientists Arnold H. Kahn and Haydn N. G. Wadley.

For information on the process sensor to measure internal temperatures in extruded aluminum, contact Haydn N. G. Wadley, A167 Materials Building, National Bureau of Standards, Gaithersburg, MD 20899, or call 301/975-6139.

INDUSTRY AND NBS JOIN IN ADVANCED CERAMICS EFFORT

NBS has agreed to cooperate with the Ceramics Advanced Manufacturing Development and Engi-

neering Center, Inc. (CAMDEC) to develop measurement technology, systems, and procedures for the processing of advanced ceramics. The establishment of CAMDEC, a not-for-profit Tennessee corporation, is the outgrowth of recommendations made by advanced ceramic leaders, including industry, at a workshop held at NBS, July 10-11, 1985, on the "Future of the U.S. Advanced Ceramics Industry." CAMDEC has as its mission the creation of a national center for developing the processing and manufacturing technology required to commercialize advanced structural ceramics. Under the agreement, NBS will provide technical advice to CAMDEC, participate in non-proprietary research and development projects, and conduct cooperative tests at NBS and CAMDEC facilities.

For information on the cooperative program, contact Stephen Hsu, A257 Materials Building, National Bureau of Standards, Gaithersburg, MD 20899, or call 301/975-6119.

NEW FEDERAL STANDARD FOR BASIC IS APPROVED

The Department of Commerce has approved a new Federal Information Processing Standard (FIPS) for the computer language BASIC. (FIPS are developed by NBS for use by the Federal Government.) The main purpose for the standard is to make it easier and less expensive to maintain BASIC programs and to transfer them among different computer systems.

The new standard, which becomes effective March 1, 1988, adopts the American National Standard for BASIC (ANSI X3.113-1987) and supersedes an earlier Federal standard (FIPS 68-1). It reflects major changes, improvements, and additions to the BASIC specifications.

For information on ordering BASIC (FIPS PUB 68-2), contact the National Technical Information Service, Springfield, VA 22161.

Standard Reference Data

NBS/EPA/MSDC MASS SPECTRAL DATA- BASE AVAILABLE FOR PC USERS

The NBS/EPA/MSDC Mass Spectral Database—a major international source of more than 44,000 analytical mass spectra—is now available from NBS for use on personal computers.

The PC version of the database was prepared from the NBS/EPA/MSDC Mass Spectral Data-

base that is in use worldwide in a computer-magnetic tape format and as a six-volume, 7,000-page reference. The collection of evaluated electron ionization mass spectra of organic and inorganic substances was originally put together by scientists at the Environmental Protection Agency (EPA) and the National Institutes of Health (NIH). It is now maintained jointly by NBS, EPA, and the Mass Spectrometry Data Centre (MSDC) in Nottingham, England.

The PC version of the standard reference database was prepared by Stephen E. Stein of NBS. Stein compressed the 44,000 spectra in the magnetic-tape version and new search programs into 13 high-density floppy disks. The database is designed to be stored on a hard disk of any AT-class or XT-class PC, where it occupies between 8 and 15 megabytes, depending on how many search options are needed by the user.

Stein designed programs which rapidly search the database either for spectra of specific chemicals according to chemical name, chemical formula, molecular weight, or Chemical Abstracts Registry Number, or for spectra which have pre-selected characteristics such as peaks at certain masses.

The PC version of the NBS/EPA/MSDC Mass Spectral Database is available for \$750 from NBS. For information on the database, or to obtain a license agreement, contact the Office of Standard Reference Data, A320 Physics Building, National Bureau of Standards, Gaithersburg, MD 20899, or call 301/975-2208.

Standard Reference Materials

AST ENZYME LEVELS CAN BE CHECKED WITH NEW MATERIALS

A reference material (RM) aimed at improving the precision of tests for elevated levels of the enzyme aspartate aminotransferase (AST) is now available from NBS. Levels of the enzyme in blood are important because, if elevated, they can indicate a variety of clinical disorders. Among these are heart attacks, congestive heart failure, hepatitis, and liver disease.

The enzyme value found in the new RM's, while not certified, was derived from an interlaboratory study in which 10 analytical laboratories participated. The new material also was produced from human blood sources. (An NBS standard reference material currently for sale, Human Serum, contains a noncertified value for AST, but the enzyme in

this case is from non-human sources.) Packaged in vials, the new reference material, Aspartate Aminotransferase (AST) (E.C.2.6.1.1)-Human Erythrocyte Source (RM 8430), is freeze-dried and intended for reconstitution with 2 milliliters of water. It contains 96.1 international enzyme units per liter, plus or minus 2.6 units. The new Reference Material is available for \$120 per set of three vials from the Office of Standard Reference Materials, B311 Chemistry Building, National Bureau of Standards, Gaithersburg, MD 20899, or call 301/975-6776.

NBS Services

NBS ELECTROMAGNETICS LABORATORY ACCREDITATION PROGRAM EXPANDED TO MEET INDUSTRIAL AND DEFENSE NEEDS

The electromagnetics laboratory accreditation program, managed by NBS under the National Voluntary Accreditation Program (NVLAP), has been expanded by the Bureau to meet requests from participating accredited laboratories, the producers of electronic equipment, and the U.S. Naval Air Systems Command.

Test methods have been added to the program to help laboratories improve the quality of their testing services on products that must meet Federal Communications Commission (FCC) approval, and to assure the quality and performance of electronic devices used in military weapons systems.

The expanded program will help the manufacturers of computers, transmitters, receivers, and industrial, scientific, and medical equipment that must be tested and approved by the FCC before it can be sold in the United States. Also, the accreditation of laboratories for military test standards is important to the national defense because it helps to assure the performance of electronic devices used in military aircraft, missiles, and ground support equipment.

NBS initially limited the electromagnetics program, established in 1986, to two test methods to gain experience with the accreditation of laboratories that perform specific tests for radio frequency emissions from computing devices (FCC Part 15J) and for telephone equipment compatibility (FCC Part 68) in accordance with FCC standards.

This program, with 16 accredited laboratories nationwide, and which now includes the first phase of a proficiency testing effort, serves as the basis for the expanded electromagnetics program.

The expanded program includes test methods for radio frequency devices, including receivers (FCC Part 15), industrial, scientific, and medical devices (FCC Part 18), and radio transmitters (FCC Part 90). At the request of the Naval Air Systems Command, NBS added a military standard (MIL STD-462) for the measurement of electromagnetic interference characteristics.

For private sector laboratories, NVLAP accreditation automatically gives them international recognition for their testing services through NBS' agreements with the United Kingdom's National Measurement Accreditation Service, Australia's National Association of Testing Authorities, and New Zealand's Testing Laboratory Registration Council. International recognition of U.S. laboratories and acceptance of test data has been a high priority of industry groups and manufacturers to aid them in exporting their products to foreign countries.

Established in 1976, NVLAP is a voluntary system whereby organizations and individuals request NBS to establish a laboratory accreditation program. On an individual basis, laboratories seek accreditation for having the competence to use specific test methods.

Currently, approximately 200 laboratories are accredited in programs administered by NBS for thermal insulation, carpet, solid-fuel room heaters, acoustical testing services, personnel radiation dosimeters, commercial products (paint and paper), building seals and sealants, construction materials testing services, and electromagnetic compatibility and telecommunications equipment testing. Other programs have been proposed for asbestos hazard abatement testing, electrical and safety testing, plumbing fixture fittings testing, and computer network interface protocol testing.

Laboratories interested in accreditation for any of the test methods offered under the expanded electromagnetics program, or for information on NVLAP, should contact: Harvey W. Berger, Manager, National Voluntary Laboratory Accreditation Program, A531 Administration Building, National Bureau of Standards, Gaithersburg, MD 20899, telephone: 301/975-4016.

Transient Impact Response of Thick Circular Plates

Volume 92

Number 6

November–December 1987

Mary Sansalone and
Nicholas J. Carino

National Bureau of Standards
Gaithersburg, MD 20899

The finite element method was used to study the transient response of thick circular plates subjected to point impact. The response of plates having different geometries and subjected to impacts of different duration was studied in both the time and the frequency domains. It is shown that the transient plate response is composed of a number of different modes of vibration including P- and S-wave thickness modes, anti-symmetric flexural modes, the rod mode, and P- and S-wave diameter modes. The origin of the diameter

modes is discussed. Excellent agreement was found between the calculated frequency values and those obtained from finite element analyses.

Key words: finite element analysis; frequency spectrum analysis; Green's function; impact; stress wave propagation; transient plate response; vibration.

Accepted: January 9, 1987

Introduction

This paper presents a finite element study of the transient response of unsupported, thick circular plates subjected to elastic point impact at the center of the top surface. Green's function solutions exist to determine the transient response of an infinite plate to a point force [1,2], and several methods exist to determine the natural frequencies and mode shapes for the axially symmetric, flexural vibrations of thick circular plates with free boundaries [3,4]. Natural frequencies and modes shapes of both symmetric and antisymmetric modes of vibration of circular plates have also been determined experimentally [5]. In this paper it is shown that the transient response of a free circular plate is composed of the Green's function solution for point impact on an infinite plate and the axisymmetric modes of vibration of a circular plate, plus a

number of other resonant frequencies. The surface response of the circular plate is studied in both the time domain and the frequency domain. Changes in the response due to changing the relative dimensions of the plate, the point where the response is monitored, and the duration of the impact are discussed.

An explicit, two-dimensional finite element code (DYNA2D) developed at Lawrence Livermore Laboratories for solving finite deformation, dynamic contact-impact problems [6,7] was used to perform the numerical analyses. The reader is referred to references [8–10] for background information on transient wave propagation in a plate subjected to point impact and on the use of the finite element method for studying the transient response of bounded solids.

Plate Response

Figure 1 shows a schematic representation of point impact on a circular plate. In experimental studies carried out at NBS [8,11], point impact is generated by dropping a small steel sphere onto the

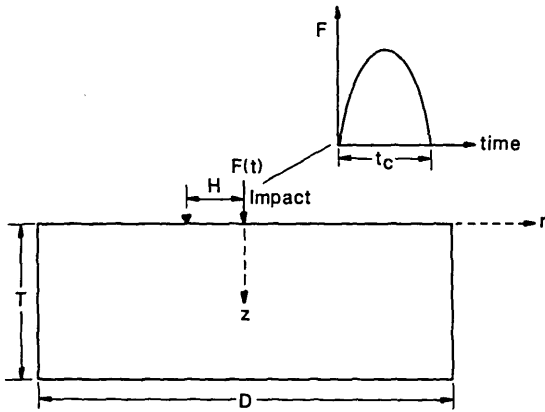


Figure 1. Schematic representation of point impact on a circular plate.

top surface of the plate. The time-history of the contact force created by the elastic impact of a sphere on a large plate can be approximated as a half-cycle sine curve [12]. For this problem, the important variables affecting the plate response are the diameter, D , and the thickness, T , of the plate and the contact time of the impact, t_c . A convenient parameter used to characterize geometries is the diameter to thickness (D/T) aspect ratio. In this study, plates with aspect ratios of 4, 5, and 6.4 were analyzed. The dimensions of each plate are given in Table 1. The contact time of the impact determines the frequency content of the stress pulse generated by the impact. In this study, contact times of 25 and 62 microseconds were used. These values are typical of those produced when small diameter steel spheres (5-10 mm) are dropped onto concrete. For 25 and 62 microsecond duration impacts, most of the energy in the stress pulse is contained in frequencies that are less than 60 and 24 kHz, respec-

tively. These values are obtained from the value of the first zero that occurs in the spectrum of the impact force-time function. This spectrum is a multi-lobed function with zeroes at $1.5/t_c$, $2.5/t_c$, $3.5/t_c$, etc. [13].

Infinite Plate Response

Before considering the response of a circular plate to impact by a sphere, the Green's function solution for point impact on an infinite plate is discussed. The Green's function is the fundamental solution to the partial differential equations and the associated boundary conditions governing elastic wave propagation. Explicit formulae which are amenable to numerical computations have been derived only for simple geometries, such as a semi-infinite space or an infinite plate. The Green's function for an infinite plate subjected to a transient point load was obtained using a computer code recently developed at NBS [2]. The Green's function solution is the normal displacement (z -direction in fig. 1) at a point on the surface of a plate caused by a step-function point force applied normal to the top surface of a plate. To obtain the response of the plate to impact by a sphere, the derivative with respect to time of the Green's function is computed. The convolution of the resulting function with the force-time function (in this case, a half-cycle sine curve), produces the desired theoretical displacement waveform.

Figure 2(a) shows the predicted normal surface displacement of a point located a distance, H equal to 0.05 m away from the point of impact on the top surface of a 0.25-m thick plate ($H/T=0.2$). The duration of the impact was 62 microseconds. For this analysis, the P-wave speed, C_p , was 4000 m/s and the ratio of S- to P-wave speeds was 0.61. In general, the computed response consists of displacements caused by the arrival of the R-wave traveling along the surface of the plate and P- and S-waves multiply reflected and mode-converted between the top and bottom surfaces of the plate.

Table 1. Frequency values for thickness, rod, flexural, and diameter modes of three circular plates (kHz)

D/T	D (m)	T (m)	Flexural ^a			Rod ^b	Thickness		Diameter ($n=4$)	
			1	2	3	4	P-Wave 5	S-Wave 6	P-Wave 7	S-Wave 8
6.4	1.6	0.25	3.5	12	20	10	8	4.9	2.1	0.65
5	1	0.2	7	22	36	15	10	6.1	3.3	0.95
4	2	0.5	4.3	10	16	7.5	4	2.4	1.7	0.43

^a Approximate for $D/T=4$ and 6.4 [4].

^b Approximate [5].

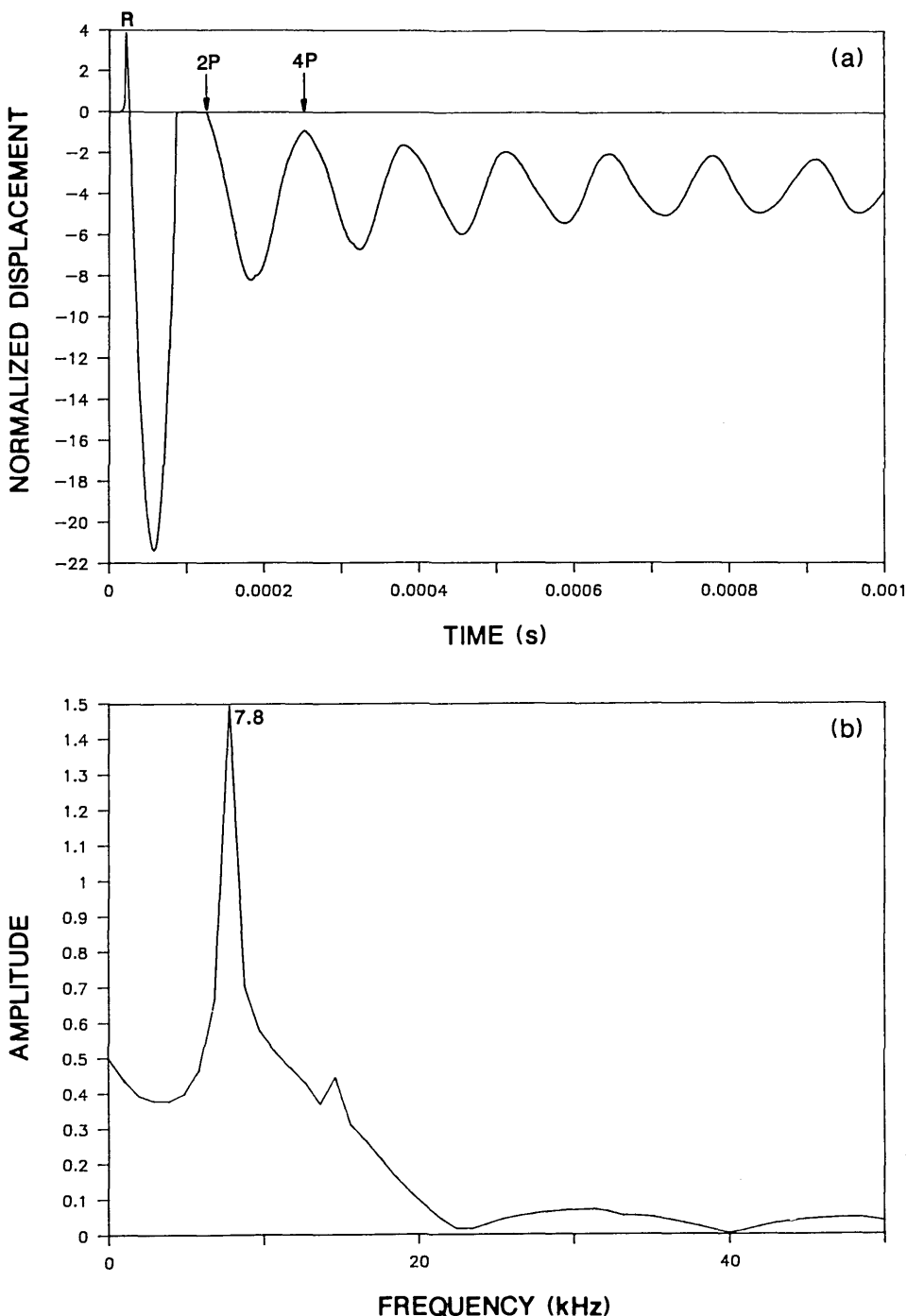


Figure 2. Green's function solution for a 0.25-m thick infinite plate subjected to a 62-microsecond duration impact: a) normal displacement waveform for a point on the plate surface located 0.05 m from the impact point; and, b) spectrum.

For this particular test condition (relatively close spacing between the impact point and response location) and for the relatively long duration impact, the surface displacement response is characterized by the displacement caused by the initial large

amplitude R-wave and a series of downward dips caused by the successive arrivals of the P-wave as it is reflected between the top and bottom surface of the plate. The arrival times of the multiply reflected P-wave are indicated as 2P, 4P, 6P, etc.

Figure 2(b) shows the spectrum obtained by taking the Fast Fourier Transform of the displacement waveform shown in figure 2(a). The digital time domain waveform consisted of 512 points and the sampling rate was 2 microseconds. Therefore, the difference between adjacent points in the spectrum was 0.98 kHz. The single large amplitude peak which occurs at 7.8 kHz in the digital spectrum¹ is the frequency of successive P-wave arrivals in the displacement response. This resonance will be referred to as the P-wave thickness mode. For points close to the impact point, this frequency is equal to the P-wave speed divided by twice the thickness of the plate ($f=C_p/2T$). For a detailed discussion of the spectra obtained from infinite plates subjected to point impact, the reader is referred to [13].

Circular Plate Response

To see how the infinite plate response is altered by the presence of the boundaries in a circular plate, the Green's function solution shown in figure 2 is compared with the response obtained from a finite element analysis of a 0.25-m thick, 1.6-m diameter, unsupported plate ($D/T=6.4$). The impact point is at the center of the top surface of the plate. Figure 3(a) shows the normal surface displacement of a point located a distance of 0.05 m ($H/T=0.2$) from the impact point. The duration of the impact was 62 microseconds. Thus the conditions are the same as for the infinite plate. Notice that the initial portion of the circular plate response (0 to 400 μ s) is similar to the Green's function solution. However, once waves reflected and mode-converted from the side boundary of the plate arrive at the response point, their effects are superimposed upon the displacements caused by waves reflected between the top and bottom surfaces of the plate.

Figure 3(b) shows the spectrum obtained from the displacement response shown in figure 3(a). The numbers associated with each peak correspond to mode numbers which will be described subsequently. The displacement waveform is composed of 512 points and the sampling interval is 4.7 microseconds; thus, the difference between adjacent points in the amplitude spectrum is 0.42 kHz. Prior to performing the Fast Fourier Transform, the waveform was shifted so that the displacement response exhibited approximately equal areas above and below the zero line. This shift was carried out by subtracting a ramp function from the

displacement response. This ramp function was equal to zero at time zero. This was done to eliminate the large zero frequency component in the spectrum caused by the rigid body translation of the unsupported plate. This shift was performed on all the waveforms shown in this paper.

As expected from the displacement response in figure 3(a), the spectrum is more complicated than the spectrum obtained from the infinite plate. The peak at 7.9 kHz due to the P-wave thickness mode (labeled as mode No. 5) is now just one of a number of peaks present in figure 3(b). (Note that the relative amplitude of the peaks present in a spectrum will depend in part on the length of the displacement response.)

To help explain the spectrum obtained from this plate and from the other plates discussed in this paper, the frequencies of the known modes of vibration of a circular plate with a free boundary were determined from the published results of Hutchinson [4] and McMahon [5]. For each plate studied, table 1 lists the frequencies of the P-wave thickness mode, the first three flexural modes calculated by Hutchinson, and the rod mode observed by McMahon. All the flexural and rod mode frequencies, except for the flexural modes of the plate with an aspect ratio of 5, were obtained from Hutchinson's and McMahon's results by interpolation because their studies were generally done for plates having Poisson's ratios other than the value of 0.2 used in this study. Thus the frequency values are approximate, but fairly accurate, as the change in frequency with Poisson's ratio is nearly linear [4].

For the 0.25-m thick plate, table 1 lists frequency values of 3.5, 12, and 20 kHz for the first three flexural modes and a value of 10 kHz for the rod mode. These modes are identified as Nos. 1, 2, and 3 for the three flexural modes and No. 4 for the rod mode. The spectrum in figure 3(b) has peaks at 3.3 kHz (mode No. 1), 12 kHz (mode No. 2), and 9.6 kHz (mode No. 4). These values agree with the first two flexural modes and the rod mode. The third flexural mode is absent, because the 62-microsecond duration impact introduces little energy in the range of frequencies near 20 kHz or higher; therefore modes in this range of frequencies are not excited.

There are also a number of other large amplitude peaks present in the spectrum obtained from the 0.25-m thick plate. These modes have frequency values less than the P-wave thickness mode. There appears to be an S-wave thickness mode and modes related to P- and S-waves propagating back and forth across the diameter of the plate. Table 1 also lists the calculated values of these modes for each

¹ The theoretical value is 8 kHz; 7.8 kHz is the closest frequency in the digital spectrum.

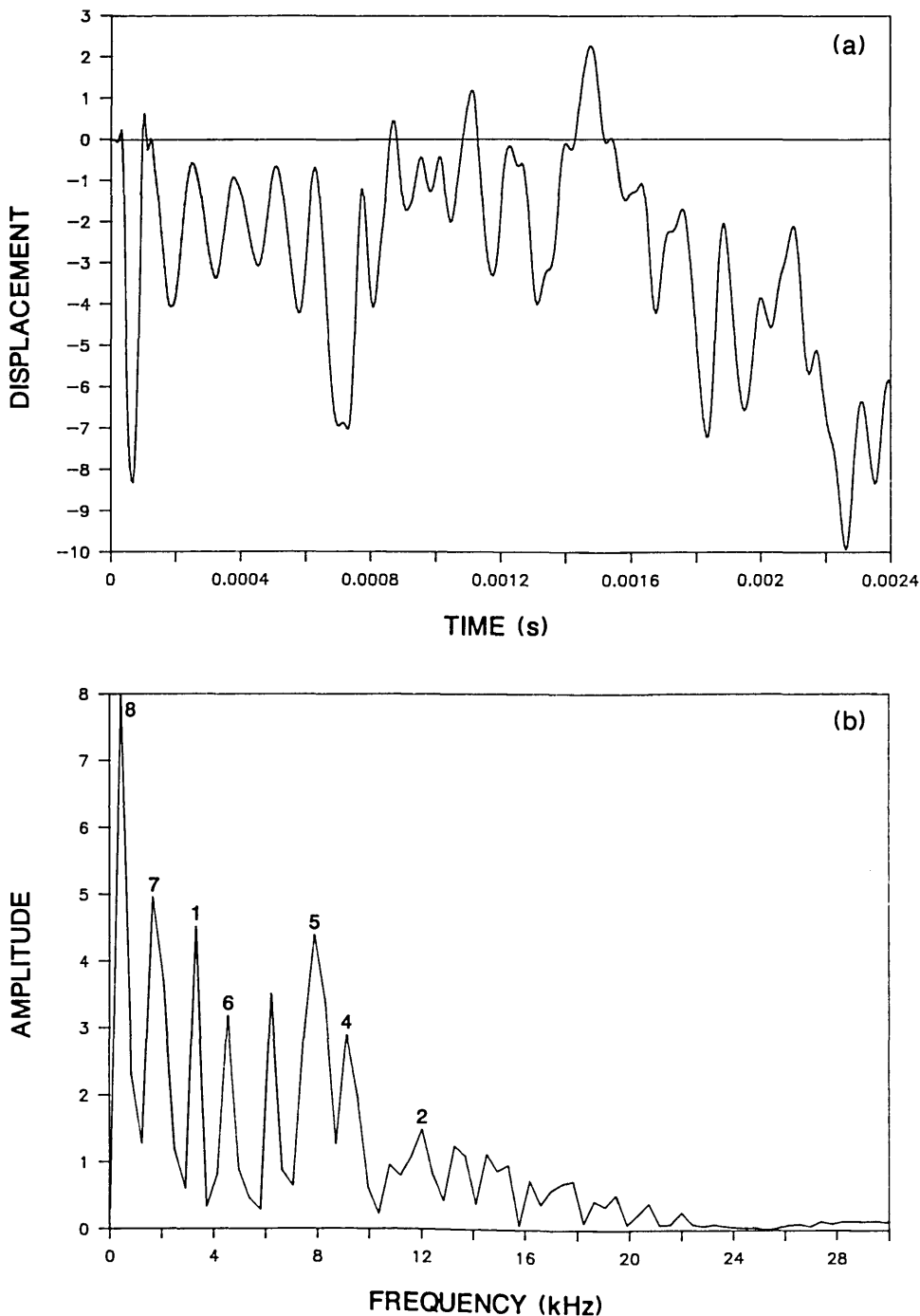


Figure 3. Finite element response of a point on the surface of a 0.25-m thick, 1.6 m diameter, plate subjected to a 62-microsecond duration impact: a) displacement waveform ($H=0.05$ m); and, b) spectrum.

plate studied. Each of these modes is discussed in the following paragraphs.

The radiation pattern for the S-wave [14-16] shows that the amplitude of displacements in the S-wave is very small in the region directly under the impact point. Thus, surface displacement re-

sponses recorded near the impact point, are dominated by displacements caused by P-wave reflections; displacements caused by S-wave reflections are often difficult to identify. Therefore, a spectrum would not be expected to exhibit a large peak at the S-wave thickness frequency. This idea is

substantiated by the spectrum obtained from the Green's function response [fig. 2(b)] which does not contain a noticeable peak at the frequency of the S-wave thickness mode (4.9 kHz). However, the spectrum obtained from the bounded plate response [fig. 3(b)] contains a peak at 4.6 kHz (labeled as mode No. 6) which agrees with the calculated S-wave thickness frequency.

In figure 3(b), the largest amplitude peaks are the frequency peaks labeled as modes No. 7 and 8. These are the P- and S-wave diameter (or radial) modes and they occur because of the presence of the side boundary of the plate. To explain these resonances, the reflection of wavefronts in a bounded plate is shown in figure 4. Impact generates spherical P- and S-wavefronts. Reflection

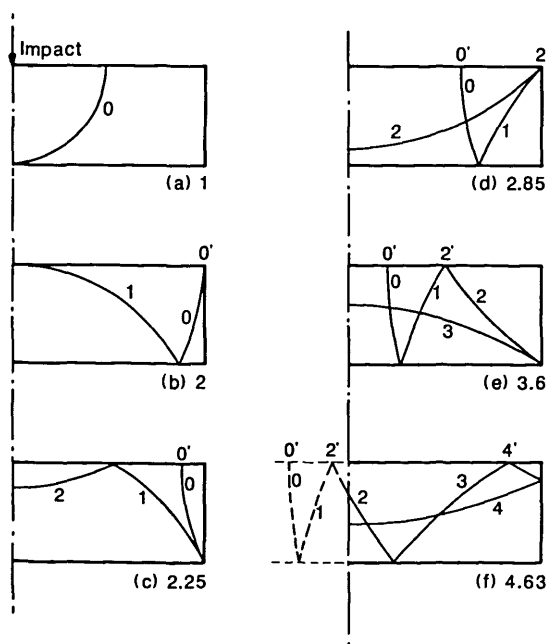


Figure 4. Location of reflected wavefronts in a circular plate at the following normalized times: a) 1; b) 2; c) 2.25; d) 2.85; e) 3.6; and, f) 4.63.

of these wavefronts at boundaries is governed by Snell's law. For simplicity only one wavefront is shown in figure 4 and mode-converted wavefronts are not shown. In addition, only that portion of the plate on one side of the centerline is shown. Each portion of the wavefront is identified by a number which corresponds to the number of times that portion has been reflected between the top and bottom surfaces of the plate. Figures 4(a) through (f) depict the location of the wavefront at successively later times after the start of an impact. These times are indicated in each figure and are nondimensionalized in terms of the time, T , it takes for the wave to travel one plate thickness.

Figure 4(a) shows the spherical wavefront spreading out into the plate; reflection from the bottom plate surface is about to begin. In figure 4(b) a portion of the wavefront, after reflection at the bottom surface, arrives back at the top surface of the plate (No. 1) and at the same time the initial wavefront (No. 0) intersects the side of the plate. As the wavefront spreads it is repeatedly reflected between the top and bottom plate surfaces, and portions of the wavefront incident on the perimeter (side) of the plate are reflected back towards the center of the plate. This reflection at the side of the plate results in a series of fronts which propagate back and forth across the diameter of the plate. Figure 4(c) shows the first portion of the front that is reflected from the side of the plate. Figure 4(d) shows the second portion of the front and figure 4(e) shows the third portion. Finally, figure 4(f) shows the fully developed fourth portion of the front and the beginning of the fifth portion. The side-reflected portions of the wavefront will propagate across the diameter of the plate to be reflected at the perimeter of the plate. Since this problem is axisymmetric, once the side-reflection portions of the wavefront pass the center of the plate they will overlap wavefronts reflected from the opposite diameter. In figure 4(f), the overlapping portions of the wavefront are shown by dashed lines.

Notice that in figure 4, the portions of the wavefront reflected from the perimeter of the plate intersect the top surface at points labeled $0'$, $2'$, and $4'$. These numbers correspond to the number of times the portion of the wavefront that intersects the top surface had been reflected through the plate thickness. A displacement response recorded on the top plate surface will include the effects produced by the arrival of these fronts. From a study of plates with different aspect ratios, it was found that it is the arrival of the P- and S-front represented by point $4'$ in figure 4(f) that gives rise to the large amplitude peaks (modes No. 7 and 8) in the spectrum. To explain why, it is helpful to think of wave reflection in terms of ray paths.

Figures 5(a) through (c) show the ray paths corresponding to the points $0'$, $2'$, and $4'$ when each of these fronts arrives at the centerline of the plate. The arrival of point $0'$ [Fig. 5(a)] is the result of a ray that travels back and forth along the top surface of the plate. The radiation patterns for the P- and S-waves show that both waves have zero amplitude in the normal direction at the surface, so the displacement caused by the arrival of point $0'$ is insignificant. The arrival of point $2'$ results from a ray that has been reflected through the thickness of the plate two times. When point $2'$ is near the

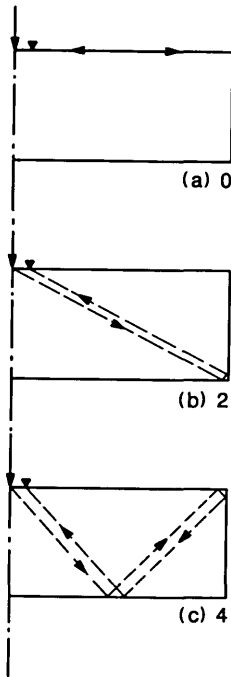


Figure 5. Ray paths corresponding to points on the wavefront: a) point 0'; b) point 2'; and, c) point 4'.

centerline of the plate, the corresponding ray path is as shown in figure 5(b). Similarly, the arrival of point 4' results from a ray that has been reflected through the plate thickness four times. When point 4' is near the centerline of the plate, the corresponding ray path is as shown in figure 5(c).

After points 2' and 4' arrive at the center of the plate, they travel towards the plate perimeter and subsequently return back to the center along the same ray paths that were shown in figures 5(b) and (c). For a point at or near the centerline of the plate, the following formula can be used to calculate the frequency of successive arrivals of points 2' and 4':

$$f_P = \frac{C_P}{[D^2 + (nT)^2]^{0.5}} \quad (1)$$

where: D = diameter of plate;
 T = thickness of plate;
 C_P = P-wave speed;
 n = number of the wavefront (2, 4, etc).

The frequencies of successive P-wave arrivals of points 2' and 4' at a point on the surface of the 0.25-m thick, 1.6-m diameter plate are 2.4 and 2.1 kHz, respectively. Peak No. 7 in figure 3(b) has a value of 1.7 kHz which is the value of the point in

the spectrum that is just less than 2.1 kHz, the computed frequency for point 4'.

When this same analysis is applied to the S-wave diameter mode, the calculated frequencies for point 4' are twice the observed frequencies. In plate displacement response it was observed (and will be shown in the next section) that the arrival of point 4' causes an upward displacement of the plate surface. The surface of the plate remains displaced upward and displacements caused by other wave arrivals are superimposed upon its general upwardly displaced shape. However, after point 4' undergoes a second reflection at the side boundary, its arrival causes a downward displacement. Again, the plate remains displaced downward until the next arrival of point 4' reverses the displacement. Thus the periodicity of displacements is twice the time it takes for point 4' on the S-wavefront to traverse the diameter of the plate. For the 0.25-m thick plate, this periodicity corresponds to a calculated frequency of 0.65 kHz. The value of the frequency peak labeled mode No. 8 in figure 3(b) is 0.42 kHz, the closest value to 0.65 kHz in the digital spectrum. The studies of plates with different dimensions show that only the frequencies calculated for point 4' agree in all cases with the frequency obtained from the finite element analyses.

Table 2 shows a comparison between the calculated frequency values for the various modes of vibration and the frequency values obtained from finite element analyses for each of the plates studied in this paper.

Aspect Ratio

Figures 6 and 7 show waveforms and spectra obtained from a 0.2-m thick plate with an aspect ratio of 5 and a 0.5-m thick plate with an aspect ratio of 4, respectively. In both cases, the duration of the impact was 62 microseconds and the response was recorded at a distance of 0.05 m from the impact point. Thus, the test conditions were the same as for the 0.25-m thick plate. The displacement waveforms for both plates were composed of 256 points and the sampling interval was 9.4 microseconds; thus the difference between adjacent points in the spectrum of each is 0.42 kHz.

In figure 6(a) the displacement waveform for the 0.2-m thick plate is shown in its linearly shifted form so that the effect of the S-wavefront propagating back and forth across the diameter of the plate can be clearly seen. For this plate, the theoretical frequency of the S-wave diameter mode is 0.95 kHz. This corresponds to a period of approximately 1000 microseconds. Notice that in the

Table 2. Comparison of calculated frequencies with frequencies based on Finite Element (FE) analyses^a (kHz)

Mode No.	Mode	0.25-m PLATE		0.2-m PLATE		0.5-m PLATE	
		$D/T=6.4$		$D/T=5$		$D/T=4$	
		Calc	FE	Calc	FE	Calc	FE
1	1st Flex	3.5	3.3	7.0	7.1	4.3	4.7
2	2nd Flex	12	12	22	^b	10	11.1
3	3rd Flex	20		36		16	
4	Rod	10	9.6	15	15	7.5	7.1
5	P Thickness	8	7.9	10	9.6	4.0	3.7
6	S Thickness	4.9	4.6	6.1	5.4	2.4	2.5
7	P Diameter	2.1	1.7	3.3	3.3	1.7	1.7
8	S Diameter	0.65	0.42	0.95	0.83	0.43	0.42

Note: Resolution in Finite Element Frequency Spectra is 0.42 kHz.

^a Contact time of the impact in the finite element analyses was 62 microseconds.

^b Frequency not identified in spectra obtained from finite element analyses.

waveform a complete cycle of alternating sets of displacements that are predominantly above and below the zero line occurs about every 1000 microseconds. This periodicity gives rise to the frequency peak of mode No. 8 (0.83 kHz) in the digital spectrum shown in figure 6(b).

The spectrum for the 0.2-m thick plate also contains peaks at frequencies that are in good agreement with the theoretical frequencies of the other modes listed in table 2. Only the frequency of the S-wave thickness mode appears slightly lower than expected. Note that the values of the second and third flexural modes for this 0.2-m plate are too high to be excited by the 62-microsecond duration impact.

Figures 7(a) and (b) show results for the 0.5-m thick plate. Again, table 2 shows that there is good agreement with the theoretical values obtained for the various modes of vibration. In this plate, the frequency of the S-wave thickness mode agrees with the theoretical value, but the amplitude of the peak is very low.

Location of Point Where Response is Recorded

Plate response is the superposition of many modes of vibration. The response changes depending on where the displacement is monitored for the following reasons: First, as the distance from the impact point increases, displacements caused by S-waves have a more significant effect on the response [8]. Large amplitude P-wave thickness reflections no longer dominate the initial displacement response. Second, the time lag in the response between displacements caused by pure thickness reflections and displacements caused by reflections from the side boundary of the plate is reduced. Third, the relative contribution to the response caused by each of the various flexural, rod, thickness, and diameter modes changes.

A detailed study of many points along the top and bottom surfaces of different plates showed that, in general, the response of a point contains the same major resonant frequencies, but that the relative contribution of each mode can change dramatically from point to point. Modes can disappear from the response if the point happens to be a displacement mode (point of zero displacement) for a particular mode.

It was also found that, for the same radial distance from the impact, points located on the top and bottom surfaces of the plate produced similar responses. This will be shown in the next section, where responses obtained at the center of the bottom surface of a plate (epicenter) are used to demonstrate the effects of changing the contact time of the impact.

Contact Time of the Impact

To show the effect on the plate response of the frequency content of the impact, an analysis was carried out for a 25-microsecond duration impact on the 0.2-m thick plate and compared with the response obtained for a 62-microsecond duration impact. Figures 8 and 9 show responses obtained at the center of the bottom surface of the plate (epicenter) for the 62- and 25-microsecond duration impacts, respectively. The displacement waveforms for both cases contained 256 points, with a sampling interval of 9.4 microseconds, giving a resolution in the spectrum of 0.42 kHz.

Recall that for a 62-microsecond duration impact, the first zero in the spectrum of the force-time function occurred at 24 kHz. Consequently, the response of plates subjected to this impact (figs. 3, 6, and 7) were dominated by frequencies less than approximately 24 kHz. This is also true for the epicenter response of the 0.2-m thick plate shown in figure 8. The epicenter response is similar to the

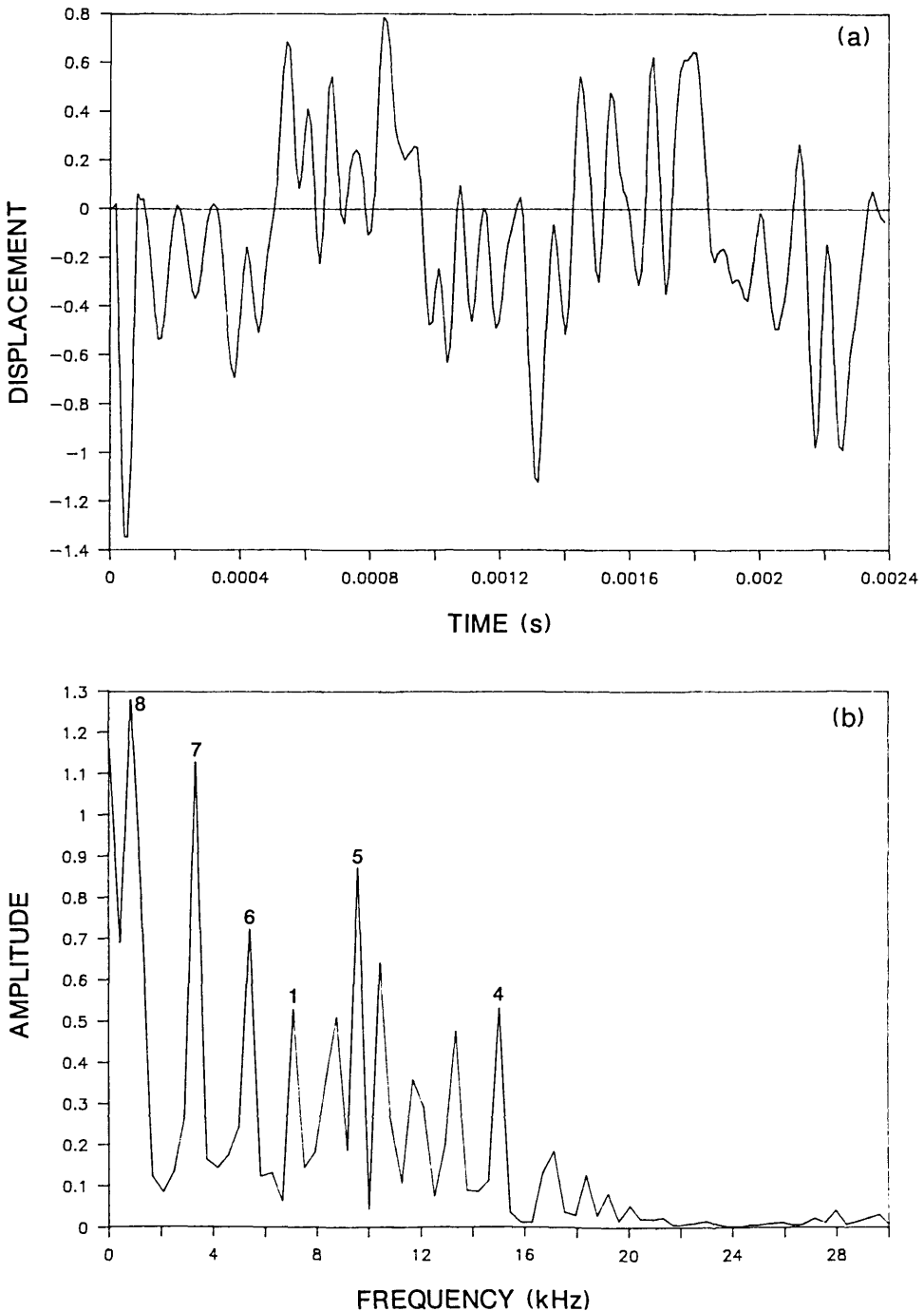


Figure 6. Finite element response of a point on the top surface of a 0.2-m thick, 1-m diameter plate subjected to a 62-microsecond duration impact: a) displacement waveform ($H=0.05$ m); and, b) spectrum.

response of a point located near the center of the plate on the top surface (fig. 6).

The 25-microsecond duration impact contains energy in a much broader frequency range than the 62-microsecond duration impact. This broader

frequency range is evident in both the waveform and the spectrum shown in figure 9(a) and (b). The displacement response in figure 9(a) contains more high frequency components which make it much more jagged than the waveform shown in figure

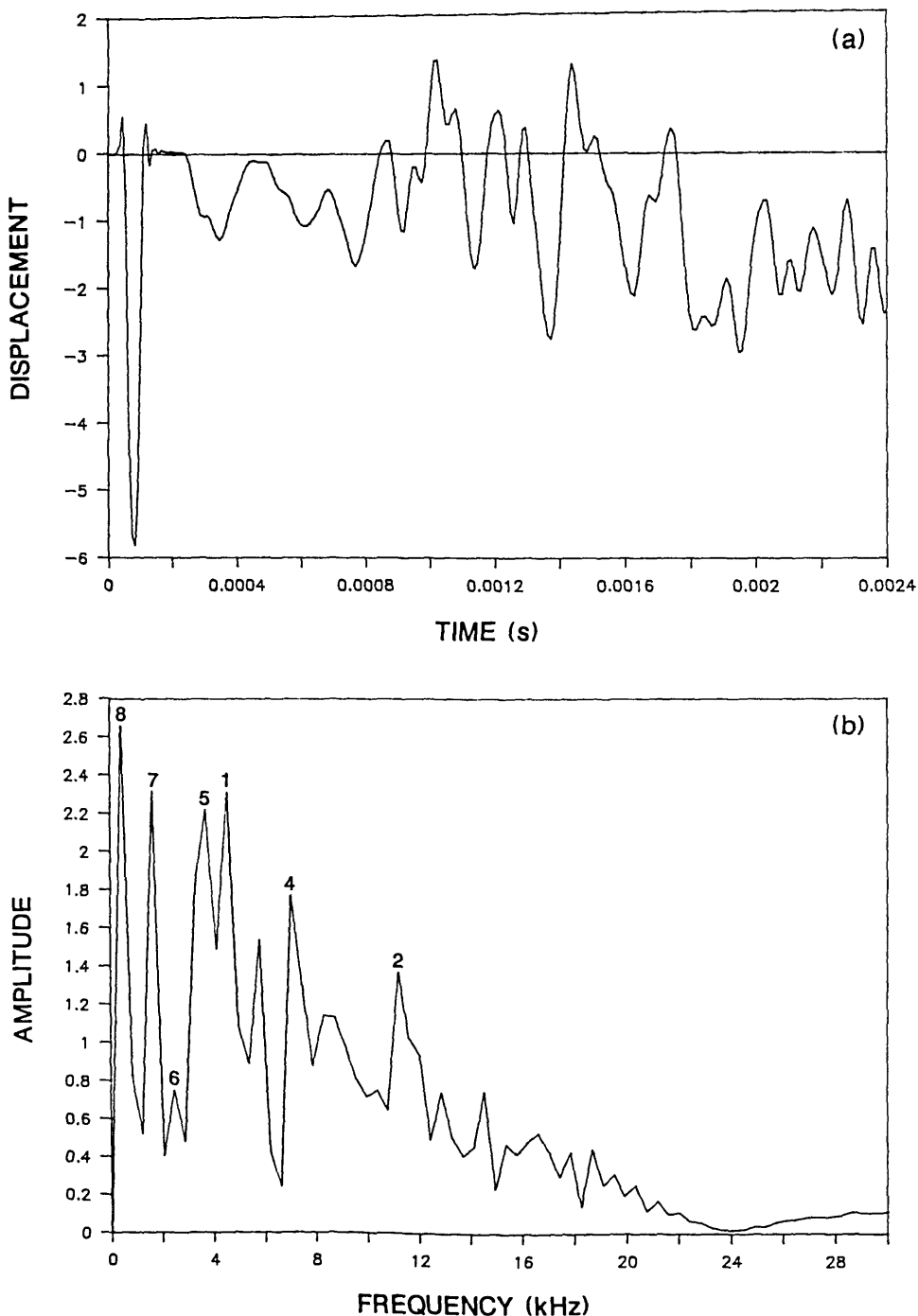


Figure 7. Finite element response of a point on the top surface of a 0.5-m thick, 2-m diameter plate subjected to a 62-microsecond duration impact: a) displacement waveform ($H=0.05$ m); and, b) spectrum.

8(a). The lower frequency portion of the spectrum (below 20 kHz) contains the same frequency peaks appearing in figure 8(b); however, the spectrum also exhibits high amplitude peaks at frequencies in the range of 20 to 40 kHz. The second and

third flexural modes produce peaks near 22 and 36 kHz. The relative amplitude of the rod mode (No. 4) at 15 kHz also increases significantly.

There are other high frequency peaks appearing in figure 9(b) that were not specifically identified.

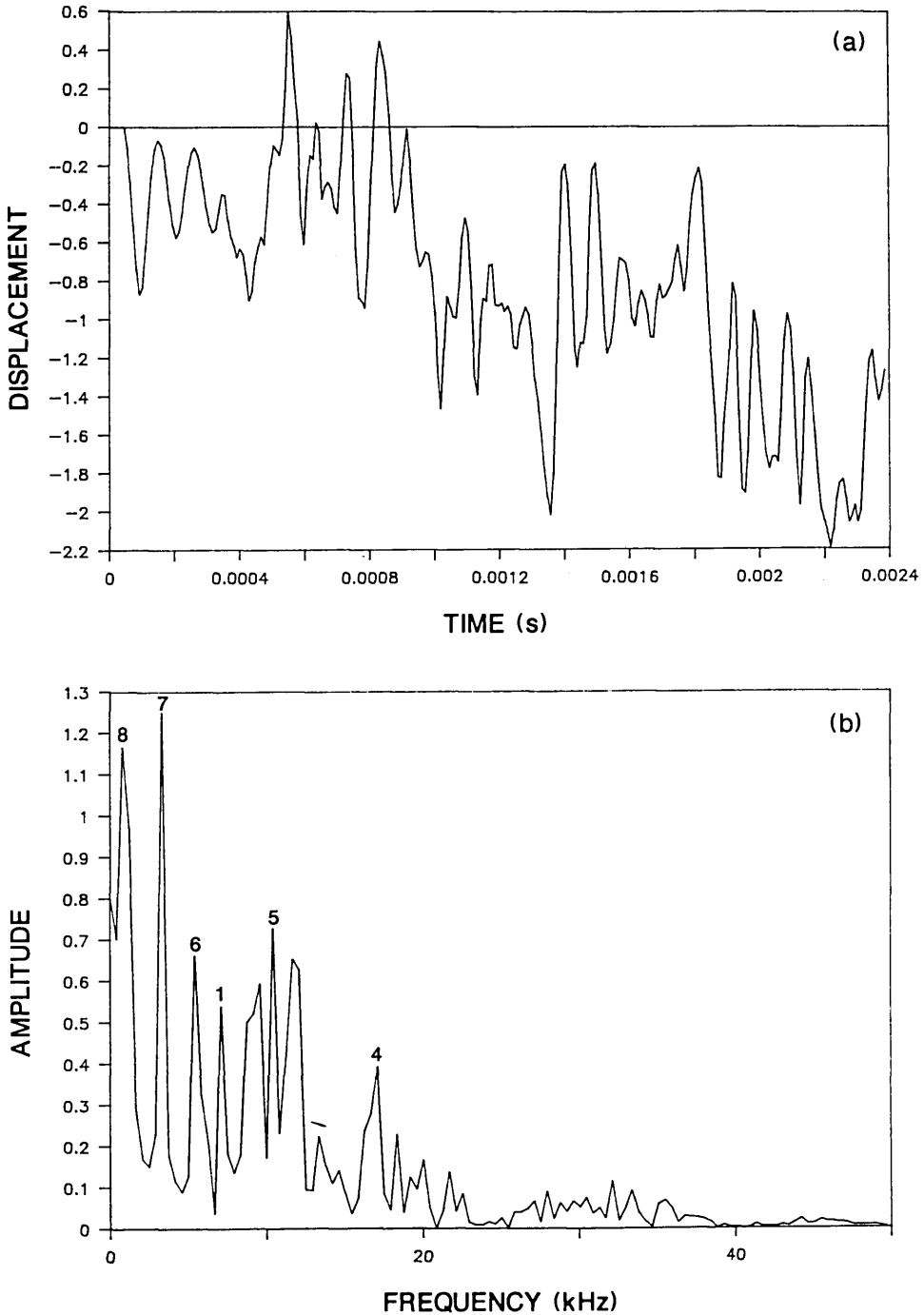


Figure 8. Finite element response at the center of the bottom surface of a 0.2-m thick plate subjected to a 62-microsecond duration impact: a) displacement waveform; and, b) spectrum.

Many of these are caused by modes of vibration which are multiples of the frequencies already discussed. Thus the shorter duration impact results in a more complicated response as higher modes of vibration in the plate are excited.

Conclusions

The primary purpose of this study was to obtain and understand the transient response of thick circular plates subjected to point impact. No theoretical solutions are available for this type of problem;

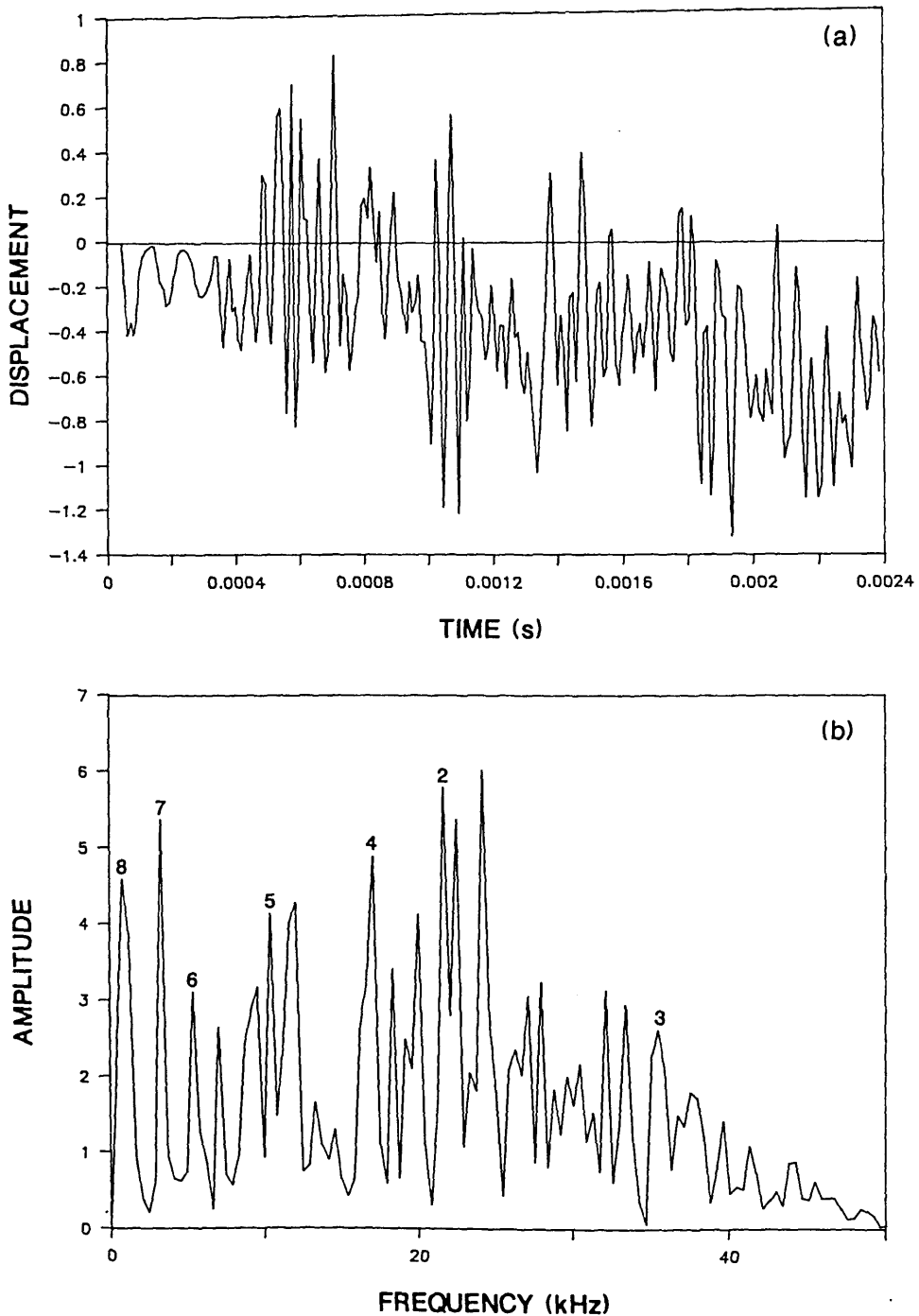


Figure 9. Finite element response at the center of the bottom surface of a 0.2-m thick plate subjected to a 62-microsecond duration impact: a) displacement waveform; and, b) spectrum.

therefore, the finite element method was used to carry out this work.

It was shown that the initial response of a circular plate is similar to the response of an infinite plate until the arrival of reflections from the perimeter of the plate complicates the response.

It was also shown that the circular plate response is due to the superposition of various modes of vibration. For the plate geometries and impact conditions studied, the response exhibited strong P- and S-wave thickness modes, flexural modes, the rod mode, and P- and S-wave diameter modes. The

origin of the diameter modes was discussed. Excellent agreement was found between the calculated frequency values of the various modes and the frequencies obtained from the finite element analyses.

Several of the variables important in impact-echo testing were considered in this study of plates. It was shown how the surface response of a plate changes with plate geometry, location where the response is recorded, and contact time of the impact. The plate responses obtained during this study will be used in a subsequent paper to compare to responses obtained from similar plates containing flaws.

About the authors: Mary Sansalone and Nicholas J. Carino are with the Center for Building Technology of the NBS National Engineering Laboratory.

References

- [1] Eitzen, D., et al., Fundamental Developments for Quantitative Acoustic Emission Measurements, EPRI NP-2089, RP608-1, Interim Report, Oct. 1982, 262 pp.
- [2] Hsu, N. N., Dynamic Green's Function of an Infinite Plate—A Computer Program, NBSIR 85-3234, National Bureau of Standards, Gaithersburg, Maryland, Oct. 1985.
- [3] Deresiewicz, H., and Mindlin, R. D., Axially Symmetric Flexural Vibrations of a Circular Disk, *ASME J. Appl. Mech.* **22**, 86 (1955).
- [4] Hutchinson, J. R., Axisymmetric Flexural Vibrations of a Thick Free Circular Plate, *J. Appl. Mech.* **46**, 139 (1979).
- [5] McMahan, G. W., Experimental Study of the Vibrations of Solid, Isotropic, Elastic Cylinders, *J. Acoust. Soc. Amer.* **36**, 85 (1964).
- [6] Hallquist, J. O., A Procedure for the Solution of Finite-Deformation Contact-Impact Problems by the Finite Element Method, UCRL-52066, Lawrence Livermore Laboratory, April 1976, 46 pp.
- [7] Hallquist, J. O., User's Manual DYNA2D—An Explicit Two Dimensional Code with Interactive Rezoning, Lawrence Livermore Laboratory, Rev. January 1984.
- [8] Sansalone, M., and Carino, N. J., Impact-Echo: A Method for Flaw Detection in Concrete Using Transient Stress Waves, NBSIR 86-3452, September 1986, 222 pp.
- [9] Sansalone, M., Carino, N. J., and Hsu, N. N., A Finite Element Study of Transient Wave Propagation in Plates, *J. Res. Natl. Bur. Stand. (U.S.)* **92**, 267 (1987).
- [10] Sansalone, M., Carino, N. J., and Hsu, N. N., A Finite Element Study of the Interaction of Transient Stress Waves with Planar Flaws, *J. Res. Natl. Bur. Stand. (U.S.)* **92**, 279 (1987).
- [11] Carino, N. J., Sansalone, M., and Hsu, N. N., A Point Source—Point Receiver Technique for Flaw Detection in Concrete, *J. Amer. Concrete Inst.* **83**, 199 (1986).
- [12] Goldsmith, W., *Impact: The Theory and Physical Behavior of Colliding Solids*, Edward Arnold Press, Ltd., 1965, pp. 24-50.
- [13] Carino, N. J., Sansalone, M., and Hsu, N. N., Flaw Detection in Concrete by Frequency Spectrum Analysis of Impact-Echo Waveforms, in *International Advances in Nondestructive Testing*, W. J. McGonnagle, Ed., Gordon & Breach Science Publishers, New York, 1986.
- [14] Miller, G., and Pursey, H., The Field and Radiation Impedance of Mechanical Radiators on the Free Surface of a Semi-Infinite Solid, *Proc. Roy. Soc. London, A* **223**, 521 (1954).
- [15] Miller, G., and Pursey, H., On the Partition of Energy Between Elastic Waves in a Semi-Infinite Solid, *Proc. Roy. Soc. London, A* **223**, 55 (1955).
- [16] Roderick, R., Radiation Pattern from a Rotationally Symmetric Stress Source on a Semi-Infinite Solid, Part II of Ph.D. Thesis, Graduate Division of Applied Mathematics, Brown University, 1951, pp. 1-29.

Transient Impact Response of Plates Containing Flaws

Volume 92

Number 6

November–December 1987

Mary Sansalone and
Nicholas J. Carino

National Bureau of Standards
Gaithersburg, MD 20899

The finite element method was used to study the transient response to point impact of thick circular plates containing disk-shaped flaws. The response was studied in both the time and the frequency domains, and compared to the response obtained from a solid plate. The effects on the response caused by changing the diameter and depth of a flaw, the duration of the impact, and the position where the response is calculated were determined. From the results of these parameter studies, conclusions were drawn which can be used

in planning and interpreting impact-echo laboratory and field test results.

Key words: finite element analysis; flaw; frequency spectrum analysis; impact; impact-echo method; nondestructive testing; stress wave propagation.

Accepted: January 9, 1987

Introduction

The results of axisymmetric, finite element studies of the transient response of thick, circular plates containing planar disk-shaped flaws subjected to point impact are presented in this paper. The capability of the finite element method for modeling transient stress wave propagation in elastic solids containing flaws was established in previous papers by the authors [1–4].

These studies are part of an ongoing research project at the National Bureau of Standards (NBS) which is aimed at developing a basis for a nondestructive test method for flaw detection in heterogeneous materials, such as concrete, using transient stress waves [1,5,6]. The experimental technique (impact-echo method) involves introducing a transient stress pulse into a test object by mechanical impact at a point. At an adjacent point, the surface displacement produced by the arrival

of reflections of the pulse from internal defects and external boundaries is monitored and the recorded waveforms are used to obtain information about the interior of a test object. Frequency spectrum analysis of waveforms is used to facilitate signal interpretation [1,6,7].

The objective of this study is to determine the effect of test variables on the ability to discern the presence of disk-shaped voids within plates from displacement waveforms and their frequency spectra. Figure 1 shows a schematic representation of point impact on a circular plate containing a disk-shaped void. A suitable point impact is generated by dropping a small steel sphere onto the top surface of the plate; the time-history of the contact force due to the elastic impact was approximated as a half-cycle sine curve (Goldsmith).

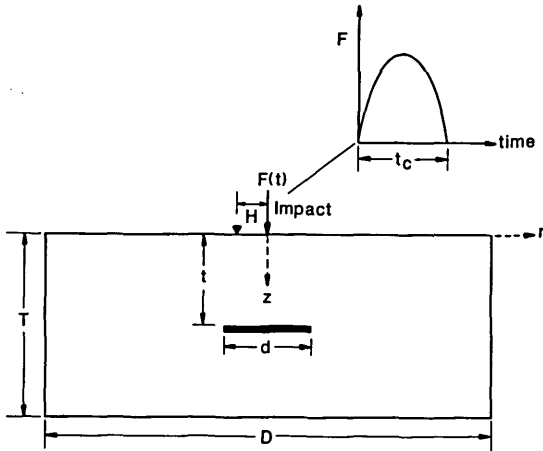


Figure 1. Schematic representation of point impact on a circular plate containing a disk-shaped void.

The important variables affecting the response of the flawed plate are: the diameter, D , and thickness, T , of the plate (D/T aspect ratio); the diameter, d , and depth, t , of the flaw; the frequency content of the stress pulse generated by impact; and, the distance, H , from the impact point to the point where the response is monitored. A study of the transient responses of unflawed circular plates of various geometries was presented in a previous paper [4]. In this study only circular plates with a diameter of 2 m and a thickness of 0.5 m were analyzed. The effect of the other variables on displacement waveforms and spectra will be discussed in this paper. Finally, it will be shown that the length of time the response is monitored, that is, the record length, is also an important factor.

Solid Plate Response

In this section, the impact response of a solid plate obtained from a finite element analysis is discussed to establish a basis for comparison to responses obtained from flawed plates. For this analysis, the elastic properties of the plate were a modulus of elasticity of 33100 MPa and a Poisson's ratio of 0.2. The density was 2300 kg/m³. These properties resulted in P-, S-, and R-wave speeds of 4000, 2440, and 2240 m/s, respectively. The impact was simulated as a pressure load over a 0.005-m diameter region at the top center of the circular plate. The time-history of the pressure was a half-cycle sine curve with a duration (contact time) of 40 microseconds.

Figure 2(a) shows a displacement waveform obtained at a point located a distance of 0.03 m from

the impact. The response consists of the following components: an initial large downward displacement caused by the Rayleigh (R) wave arrival; displacements caused by the arrival of P- and S-waves which have been multiply reflected or mode-converted between the top and bottom surfaces of the plate (e.g., the arrival of the first P-wave reflected from the bottom surface is labeled by a 2P); and finally, displacements caused by the arrival of waves reflected and mode-converted from the perimeter of the plate, which are superimposed upon the displacements caused by waves multiply reflected between the top and bottom surfaces of the plate. The R-wave has been clipped, as is normally done in laboratory studies, to accentuate the displacement caused by body waves [1,7].

Figure 2(b) shows the amplitude spectrum obtained by taking the Fast Fourier Transform of the waveform shown in figure 2(a). The waveform contained 256 points and the sampling interval was 9.4 microseconds; thus, the interval in the spectrum is 0.42 kHz. For the 40 microsecond duration impact, most of the energy in the stress waves is contained in frequencies of 37 kHz or less. This value is obtained from the value of the first zero that occurs in the spectrum of the impact force-time function [7]. Note also that before the Fast Fourier Transform of a waveform was computed, it was shifted to remove the component of the displacement caused by rigid body translation of an unsupported plate subjected to impact [4]. This shift significantly reduced the zero frequency component in the spectrum.

The spectra obtained from thick circular plates subjected to point impact exhibit peaks at resonant frequencies corresponding to the following modes [4]: waves propagating between the top and bottom surfaces of the plate (thickness modes, Nos. 5 and 6); waves propagating across the diameter of the plate (diameter modes, Nos. 7 and 8); and, flexural modes (Nos. 1-3) and the rod mode (No. 4). For each of these modes, the calculated values and the digital values from the finite element analysis are listed in table 1. All of these modes are present in figure 2(b) giving rise to a complicated response spectrum.

In the following discussion, it is shown how the presence of a disk-shaped void within the plate, depending upon its size and location, can dramatically alter the solid plate response. In all of the cases discussed in the following sections, the length and sampling interval of the time domain records, and the dimensions and material properties of the plates containing the flaws are the same as for the solid plate.

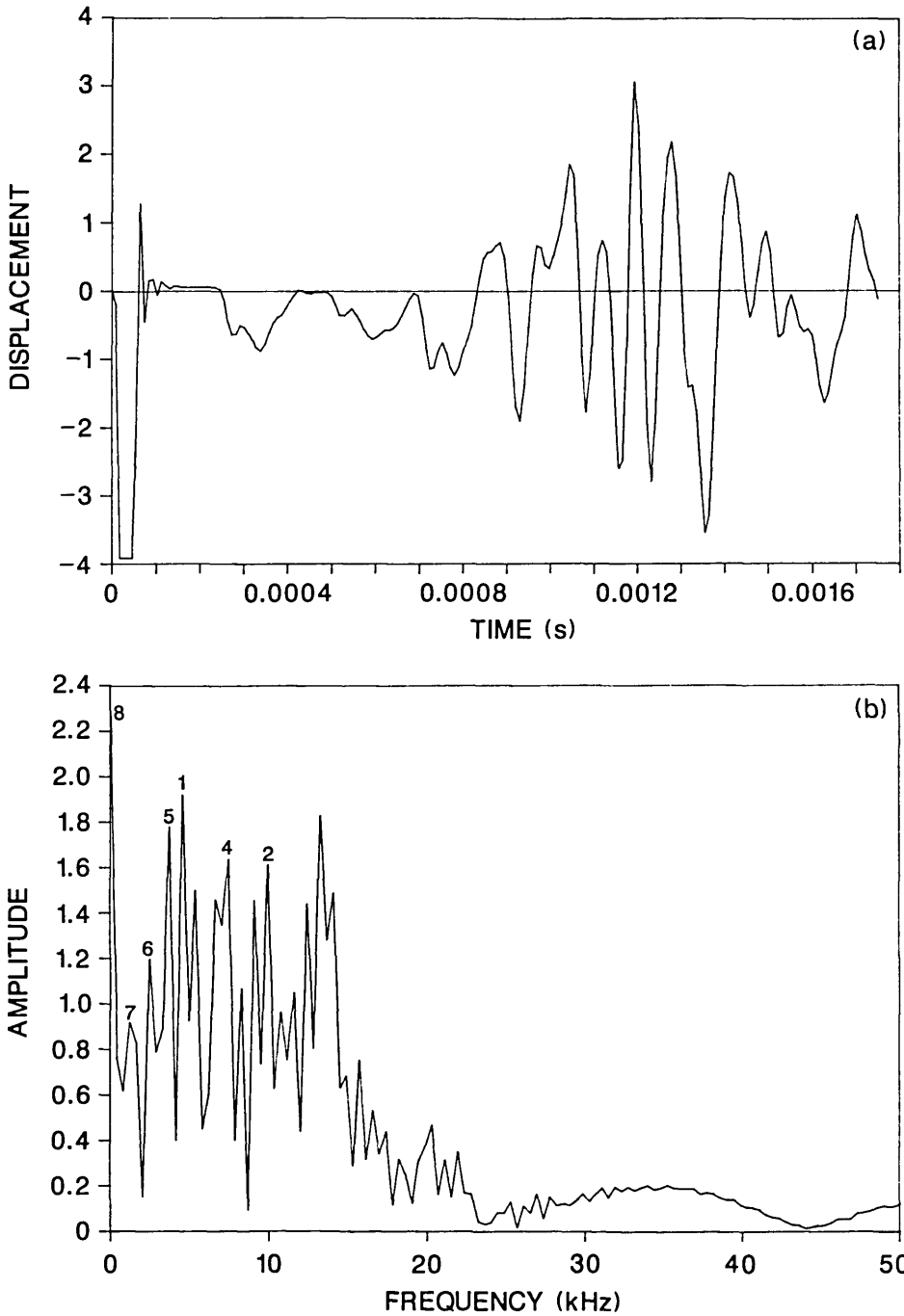


Figure 2. Finite element response of a point on the top surface of a solid 0.5-m thick, 2-m diameter plate subjected to a 40-microsecond duration impact: a) normal displacement waveform ($H=0.03$ m); and, b) spectrum.

Response of Plates Containing Flaws

Figure 3(a) shows the calculated response for a plate containing a 0.2-m diameter flaw located 0.13 m below the top surface of the plate. The flaw is a 0.01-m thick disk-shaped void. Since the prob-

lem is axisymmetric, the center of the flaw coincides with the center of the plate and the impact point is directly above the center of the flaw. The displacement was calculated 0.03 m from the impact point so that a direct comparison could be made with the solid plate results (fig. 2). The

Table 1. Comparison of calculated frequencies with frequencies based on finite element (FE) analyses^a (kHz)

Mode No.	Mode	0.5-m Plate <i>D/T=4</i>	
		Calc	FE
1	1st Flex	4.3	4.7
2	2nd Flex	10	11.1
3	3rd Flex	16	- ^b
4	Rod	7.5	7.1
5	P Thickness	4.0	3.7
6	S Thickness	2.4	2.5
7	P Diameter	1.7	1.7
8	S Diameter	0.43	0.42

Note: Resolution in finite element spectra is 0.42 kHz.

^a Theoretical values for flexural and rod modes were obtained from published analytical and experimental results [11,12].

^b Frequency not identified in spectra obtained from finite element analyses.

waveform for the flawed plate [fig. 3(a)] is very different from the response of the solid plate [fig. 2(a)] because it contains high frequency oscillations superimposed upon the plate response. These oscillations are caused by P-wave reflections between the flaw and the top surface of the plate¹.

Figure 3(b) shows the spectrum of the waveform in figure 3(a). There is a large amplitude peak at 3.76 kHz which corresponds to the frequency of P-waves that have diffracted around the edge of the flaw and been reflected from the bottom surface of the plate. (The reader is referred to refs. [1 and 3] which present detailed discussions of diffraction at the edge of a flaw.) This peak is the same P-wave thickness mode peak that was present in figure 2(b); however, in figure 3(b) the 3.76-kHz peak has a much larger amplitude compared with the remainder of the peaks in the spectrum. In figure 3(b) there is also a group of large amplitude peaks near 15 kHz. These peaks are caused by P-wave reflections from the flaw. For a P-wave speed of C_p and a flaw depth, t , the thickness mode frequency for P-waves is:

$$f = C_p / (2t), \quad (1)$$

which in this case is 15.4 kHz. Thus, reflections from the flaw produce series of frequency peaks clustered around the thickness mode frequency.

¹ Note that in figure 3(a), the high amplitude peak immediately following the downward dip due to the R-wave is caused by an overshoot response of the finite element model. This overshoot is caused by the rapid change in displacements produced by the R-wave, but it is quickly damped out using artificial viscosities [8,9].

In this case, the depth, t , of the flaw is known. If however, the depth is not known, it can be calculated from the peak frequency [eq (1)]. If the high amplitude peak at 15.9 kHz is used in equation (1), the computed depth is 0.126 m which is close to the exact depth of 0.13 m. Note that equation (1) is valid for responses measured close to the impact point.

An interesting result that appears in figure 3(b) is that the frequency peaks which are caused by resonances set up by the plate perimeter are of secondary importance [compare with fig. 2(b)]. This result is advantageous in terms of flaw detection as it allows the presence of the flaw to be easily detected and the depth of the flaw to be accurately determined.

A convenient parameter that will be used in comparisons of flaw geometries is the diameter to depth (d/t) ratio of the flaw. In this case, the presence of a flaw with a d/t ratio of 1.54 significantly altered the plate response. Before presenting results obtained from other flaw geometries, the effect of changing the contact time of the impact and of changing the location where the displacement is recorded will be discussed.

Contact Time of the Impact

The frequency content of the stress pulse produced by impact depends on the contact time of the impact [7]. A shorter contact time produces a pulse which contains energy in a broad frequency range. A longer contact time produces a pulse which primarily contains large amplitude, low frequency components. This is important because the frequency content of the waves produced by impact determines the size of the flaw that can be detected. For a flaw to be detected, it is generally stated that the dimensions of the flaw must be on the order of, or larger than, the component wavelengths in the propagating waves. For example, to detect a 0.2-m diameter flaw in concrete, frequencies in the range of 20 kHz or higher would probably be needed.

In impact-echo testing of concrete, 40- to 80-microsecond duration impacts are typical values produced by the impact of small diameter (7-12 mm) steel spheres. Figure 3 shows the response for a plate subjected to a 40-microsecond duration impact. In this case, the depth of the flaw was easily determined as a significant portion of the input energy was contained in frequencies greater than 20 kHz.

For comparison, figure 4 shows the response at the same point for an 80-microsecond duration

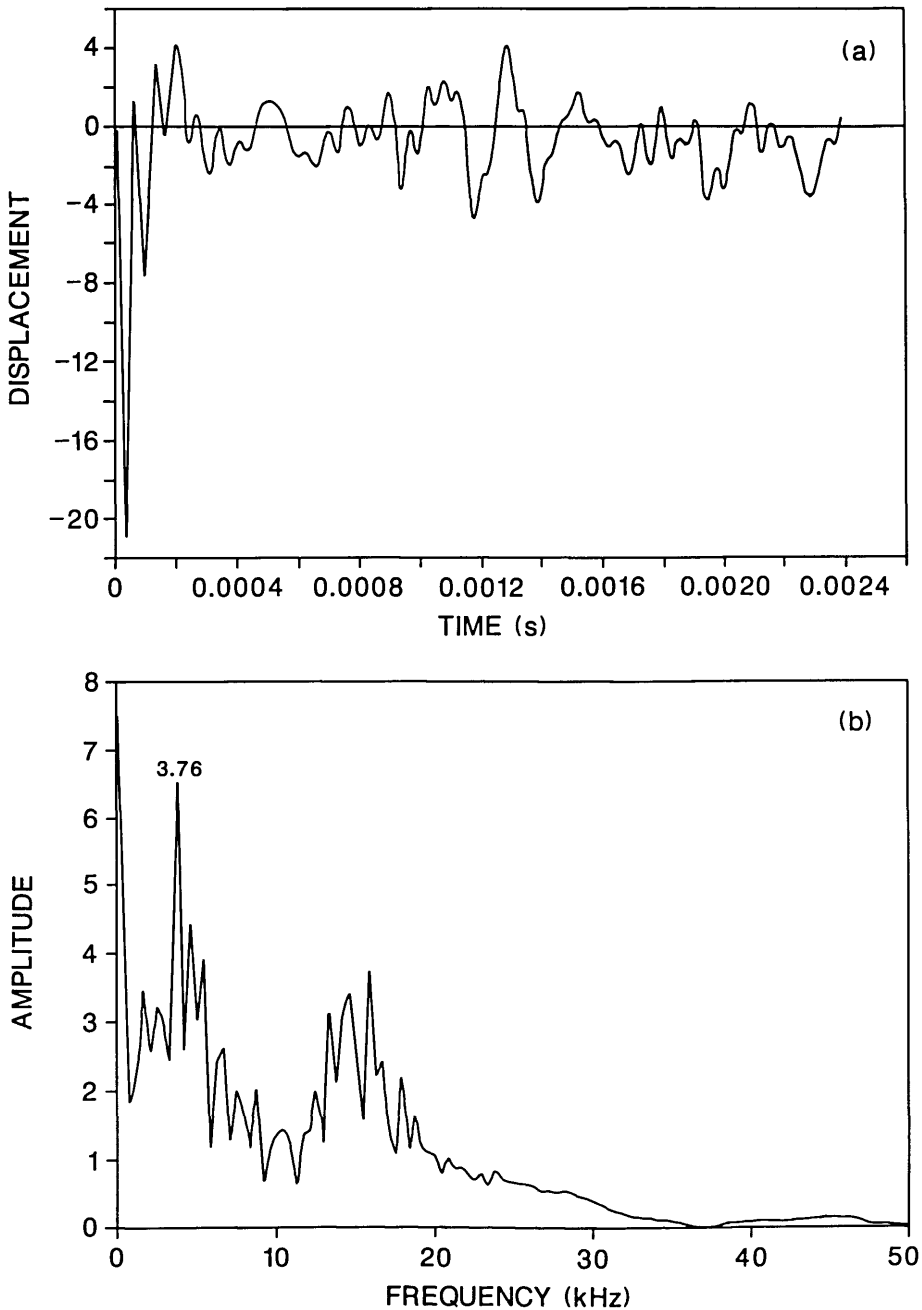


Figure 3. Finite element response of a point on the top surface of a plate containing a 0.2-m diameter flaw located 0.13 m below the top surface. The plate was subjected to a 40-microsecond duration impact: a) displacement waveform ($H=0.03$ m); and, b) spectrum.

impact on the same plate. For this contact time, most of the energy in the stress waves produced by the impact is contained in frequencies less than approximately 19 kHz. Thus, only a small amount of energy will be reflected by the flaw. The waveform in figure 4(a) does not contain the high frequency oscillations that are present in figure 3(a).

In addition, in the spectrum in figure 4(b), the peaks near 15 kHz are of very low amplitude relative to the P-wave plate thickness peak at 3.76 kHz. The depth of the flaw would be difficult to determine, however, the flaw would probably be detected, because the waveform and spectrum looks very different from that obtained from the

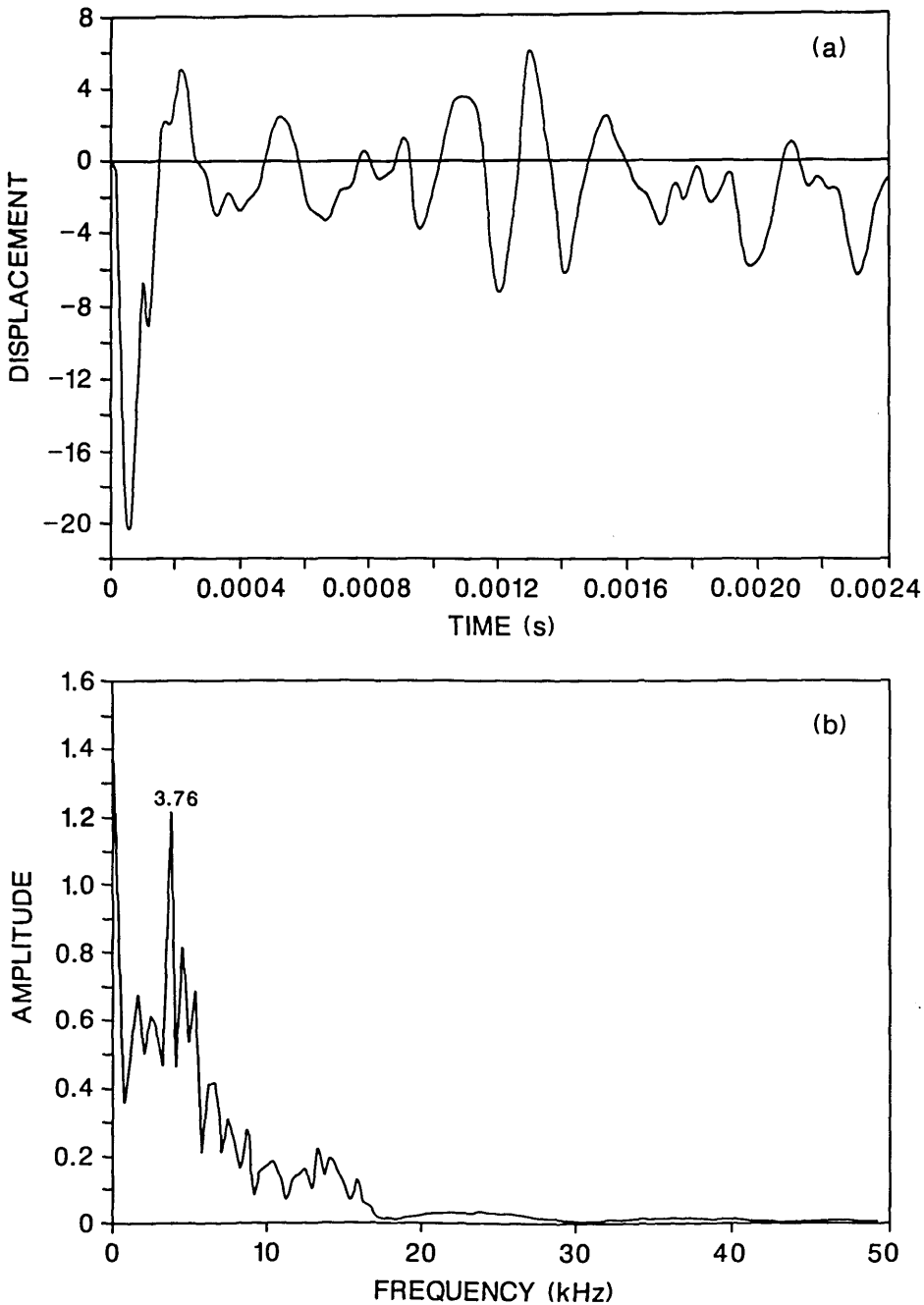


Figure 4. Finite element response of a point on the top surface of a plate containing a 0.2-m diameter flaw located 0.13 m deep. The plate was subjected to a 80-microsecond duration impact: a) displacement waveform ($H=0.03$ m); and, b) spectrum.

solid plate (fig. 2). In figure 4(a), the portion of the waveform between the R-wave and the arrival of reflections from the side of the plate shows displacements which are well above the zero displacement line. These upward displacements are caused by waves diffracted from the edge of the flaw [1,3];

they do not occur in the solid plate response [fig. 2(a)]. Also, the spectrum in figure 4(b) does not exhibit all the various plate modes that are present in the solid plate response [fig. 2(b)].

Thus the contact time of the impact is an important factor in impact-echo testing for detection of

flaws. The contact time must be chosen based on the material properties of the structure being evaluated and the size of flaw to be detected. For example, longer duration impacts must be used to penetrate heterogeneous solids such as concrete and this limits the minimum size of flaw that can be detected. These results also show that the presence of a flaw will have an effect on the plate response even if the flaw cannot be accurately located using a given impact. It should be noted that the success of the impact-echo method in laboratory and field test conditions relies on having a high fidelity transducer capable of measuring surface displacements. A transducer which has been used successfully is the conical transducer developed at NBS [10].

Location Where Response is Recorded

Surface displacement waveforms are also affected by: 1) the distance, H , between the impact point and the point where the displacement is recorded; and, 2) the location of the point where the displacement is recorded relative to the location of the flaw. It seems obvious to expect that the displacement response will be different if it is measured close to the impact point and directly over the central region of the flaw as compared to being recorded at a point that is over or off the edge of the flaw.

Figures 5 and 6 show waveforms and their corresponding spectra for the plate containing the 0.2-m diameter flaw located 0.13 m deep for values of H equal to 0.06 and 0.09 m, respectively. The duration of the impact was 40 microseconds. A comparison of the results shown in figures 5 and 6 with those shown in figure 3 ($H=0.03$ m), shows that as H increases, the high frequency oscillations due to P-wave reflections from the flaw diminish in amplitude in the waveform and there is a corresponding decrease in the amplitude of the peaks near 15 kHz in the frequency spectra. In contrast, the frequency peak produced by multiple reflections of the P-wave between the top and bottom surfaces of the plate shows only a slight decrease in amplitude.

In figures 3 and 5, the presence of the flaw can be easily detected in the waveforms and in the spectra. In figure 6, the case where the response point is nearly above the edge of the flaw, the peaks in the spectrum near 15 kHz are much lower in amplitude; however, the approximate depth of the flaw can still be determined from the single peak at 16.7 kHz. In figure 6, the presence of a flaw can also be discerned for the two reasons discussed previously: the spectrum looks very differ-

ent from that shown in figure 2 for a solid plate; and, the initial portion of the displacement waveform exhibits both high frequency oscillations and displacements that are above the zero line, indicating the presence of a sharp edge causing diffraction.

In summary, these results show that it is best to record the response near the impact point. This assures that if the impact point is over a flaw, then the maximum response caused by P-waves reflected from the flaw will be recorded and the flaw will be easier to detect and its depth easier to determine.

The discussion up to this point has focused on a plate containing a 0.2-m diameter flaw at a depth of 0.13 m—a flaw geometry with a large d/t ratio of 1.54. In the following section, the effect of changing flaw size and flaw depth will be shown.

Flaw Diameter and Flaw Depth

To show the effect of changing flaw diameter and depth, results of two analyses will be presented: 1) a plate containing a 0.07-m diameter flaw located 0.13 m below the surface of the plate (fig. 7); and 2) a plate containing a 0.2-m diameter flaw located 0.38 m below the surface of the plate (fig. 8). Both cases result in d/t values of 0.53. The duration of the impact was 40 microseconds and the displacement was calculated 0.03 m from the impact point. Thus a direct comparison can be made with the results shown in figures 2 and 3.

The initial portions of the waveforms in figures 7(a) and 8(a) show oscillations and displacements which are absent in the solid plate response [fig. 2(a)]. Therefore, the waveforms reveal that a flaw exists in both plates. Figures 7(b) and 8(b) show the frequency spectra of these waveforms; these spectra are very different from the spectrum shown in figure 3(b). In fact, they resemble the solid plate spectrum [fig. 2(b)], exhibiting a myriad of peaks corresponding to all the modal plate vibrations and resonances set up by waves propagating in the plate. However, there are differences in the frequency spectra for the plates containing the flaws as compared with the spectrum for the solid plate; these differences give indications of the presence of a flaw, but probably would go unnoticed in actual testing where the presence of a flaw was not known beforehand. In figure 7(b), there is a larger amplitude peak (as compared with figure 2(b) at 15.8 kHz which is close to the P-wave peak produced by reflections from the surface of the flaw, but this is also the frequency of the third flexural mode of the plate. Therefore, if flaw detection

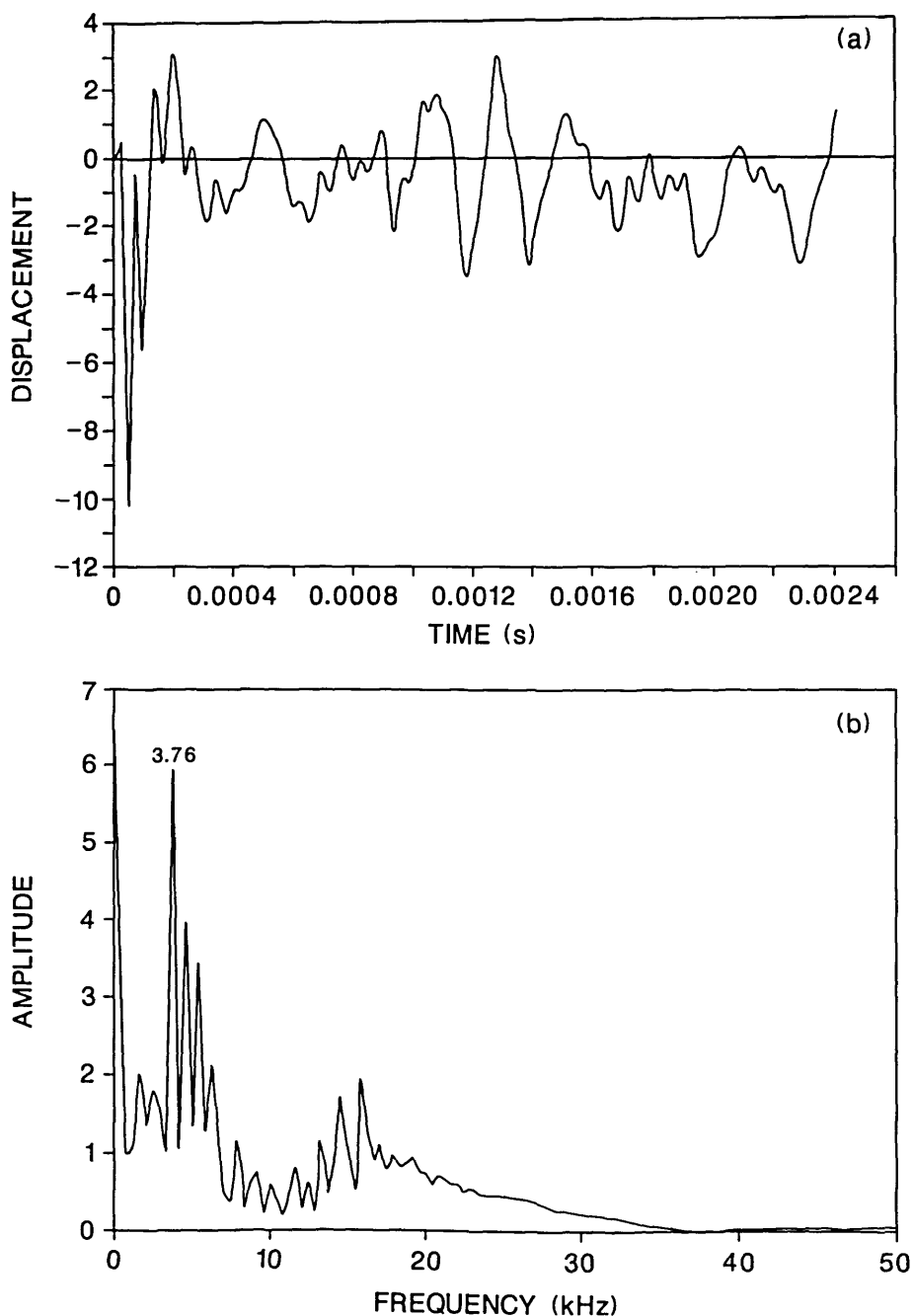


Figure 5. Finite element response of a point on the top surface of a plate containing a 0.2-m diameter flaw located 0.13 m deep: a) displacement waveform ($H=0.06$ m); and, b) spectrum.

were based solely on the spectrum, the flaw would probably not be noticed. In figure 8(b), there is a secondary peak at 5.4 kHz which is the frequency of P-wave reflections from the surface of the flaw, but this peak is also present in figure 2(b); again if only the spectrum is used, the flaw would not be detected. In these cases, the spectra are of no help

in flaw detection; however, looking at the waveforms, the effects caused by the flaws are obviously present if the displacement responses are compared to the solid plate response. As mentioned previously, in actual laboratory test conditions, this type of signal interpretation relies on having a high fidelity displacement transducer.

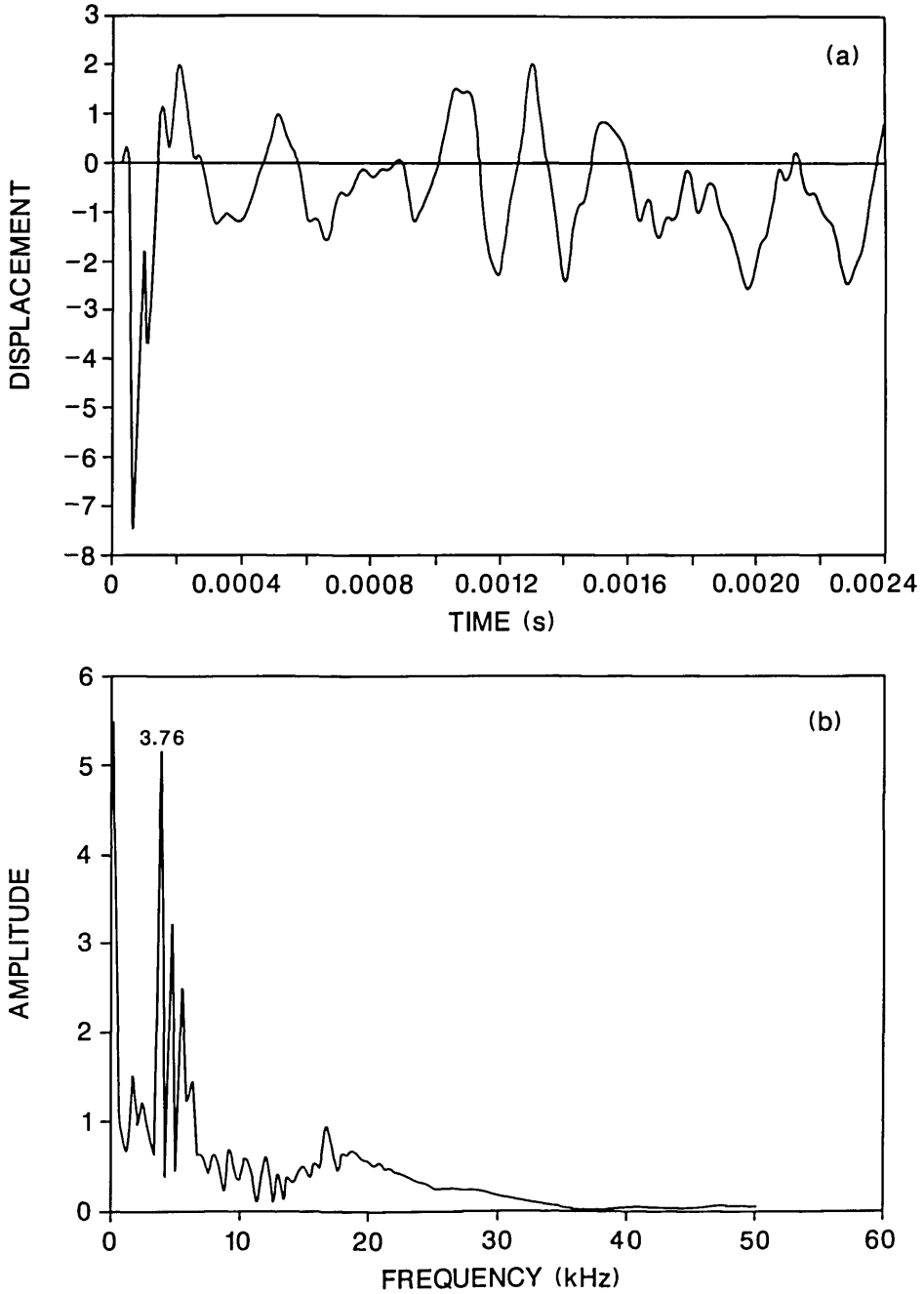


Figure 6. Finite element response of a point on the top surface of a plate containing a 0.2-m diameter flaw located 0.13 m deep: a) displacement waveform ($H=0.09$ m); and, b) spectrum.

Record Length

The effects caused by the flaws are most apparent in the early portion of the waveforms shown in figures 7 and 8. To determine the effect of record length, only the first 1200 microseconds (128 points) of each waveform was transformed. The

resulting spectra are shown in figures 9(a) and 9(b). For comparison the spectrum for the first 1200 microseconds of figure 3(a) was also obtained [fig. 9(c)]. The frequency interval in each spectrum is 0.83 kHz.

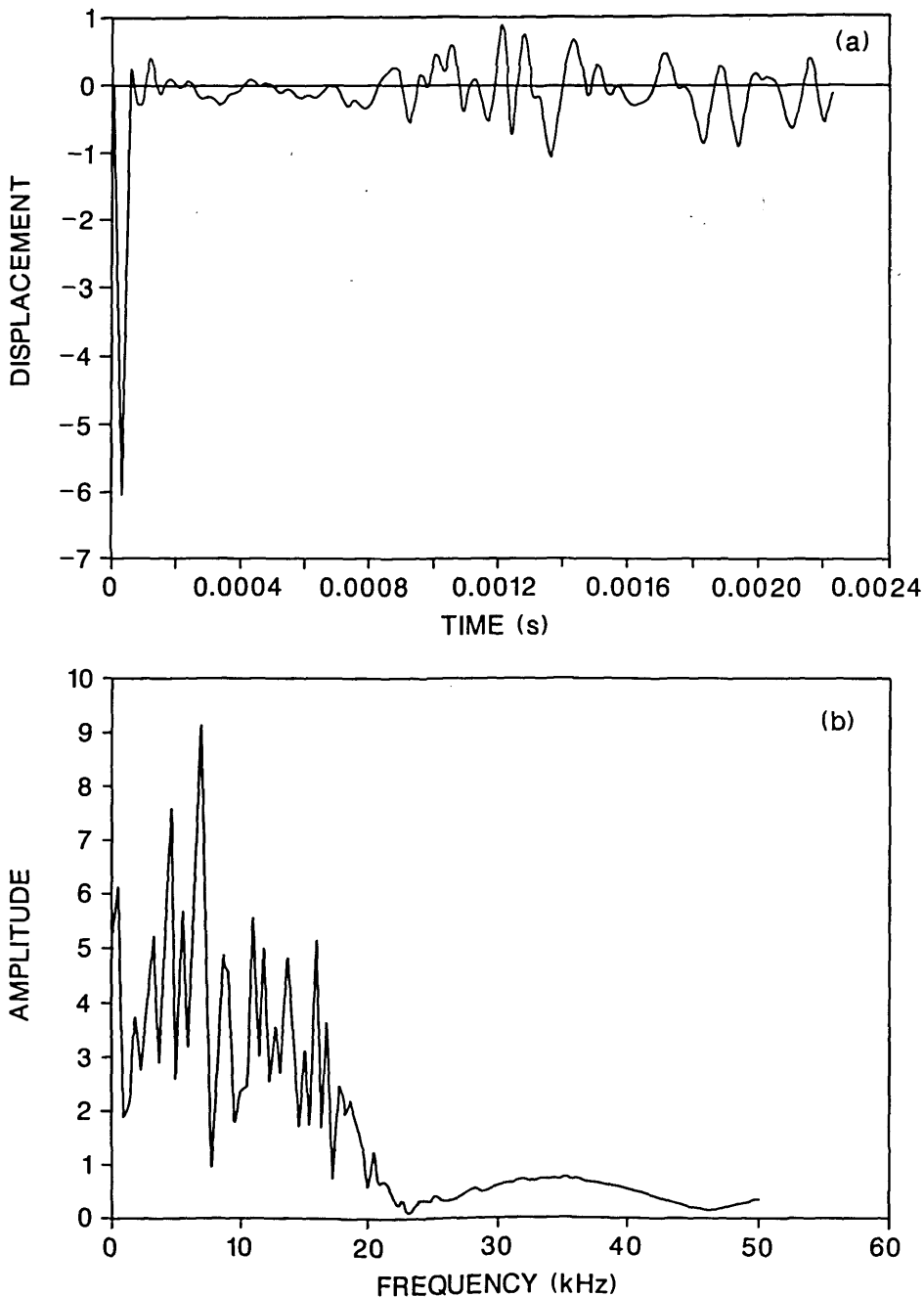


Figure 7. Finite element response of a point on the top surface of a plate containing a 0.07-m diameter flaw located 0.13 m deep: a) displacement waveform ($H=0.03$ m); and, b) spectrum.

By using only the first 1200 microseconds of the waveforms, most of the response caused by the arrival of reflections from the plate perimeter was eliminated, and the corresponding spectra clearly reveal the presence of the flaw. The spectra in figures 9(a) and (b) show the same pattern as that ob-

tained from the flaw with the large d/t value [fig. 3(b)]. There is a large amplitude peak(s) near 4 kHz caused by P-wave reflections between the top and bottom surfaces of the plate, and a second large amplitude peak caused by P-wave reflections from the surface of the flaw. In all cases, the depth of the flaw can be accurately determined.

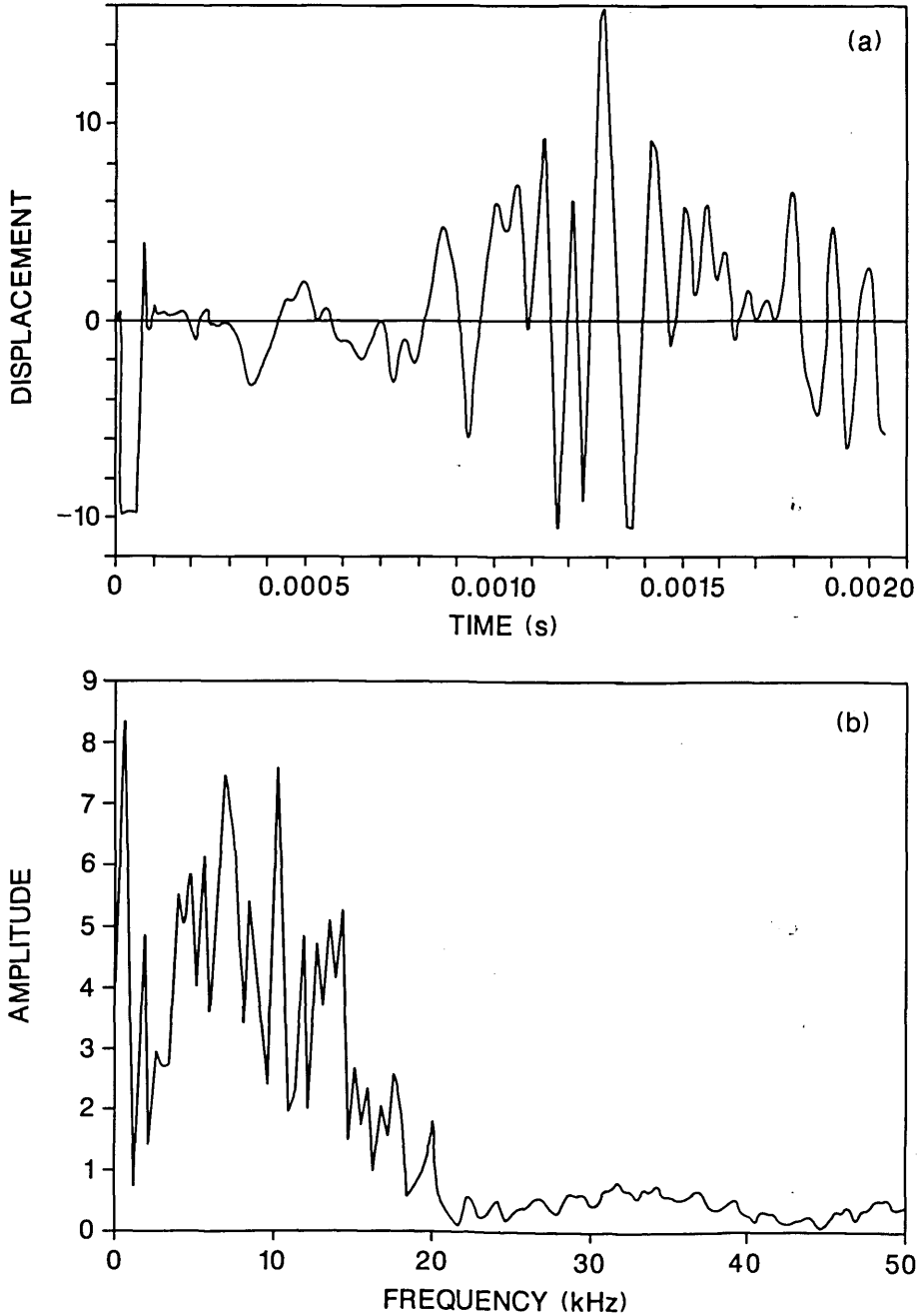


Figure 8. Finite element response of a point on the top surface of a plate containing a 0.03-m diameter flaw located 0.38 m deep: a) displacement waveform ($H=0.03$ m); and, b) spectrum.

Thus in impact-echo testing it appears to be advantageous to restrict the time-domain waveform to reflections occurring prior to multiple reflections from the side boundaries of a structure—reflections which give rise to flexural vibrations and other resonances. This is especially true for detect-

ing smaller flaws or larger flaws located deep within a structure (smaller d/t values). However, by using a shorter record length, there is an increase in the frequency interval of the digital spectrum which can lead to inaccuracy in determining the depth of a flaw.

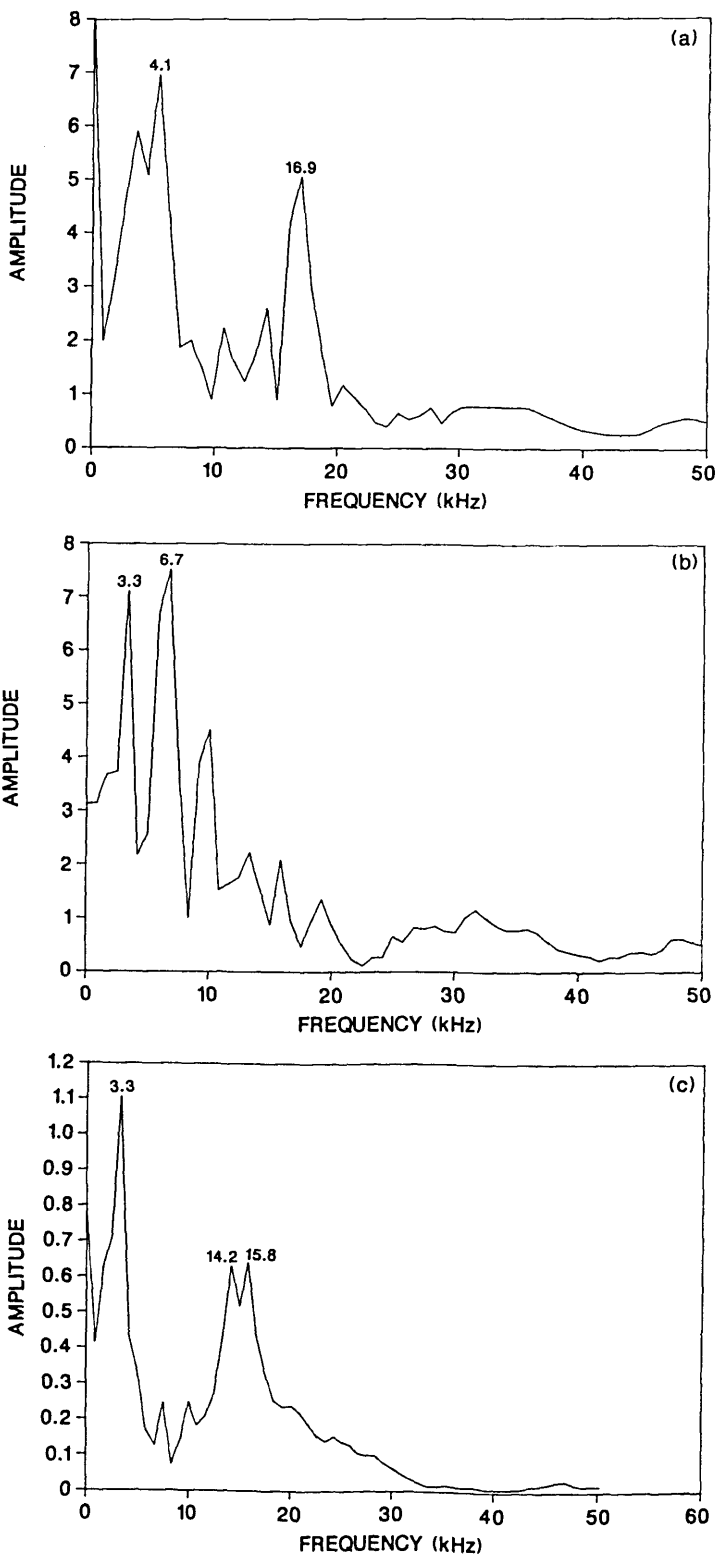


Figure 9. The effect of record length on frequency spectra. For a 1200 microsecond record length spectra were obtained from surface displacement waveforms from plates containing flaws: a) 0.07-m diameter flaw located 0.13 m deep (fig. 7); b) 0.2-m diameter flaw located 0.38 m deep (fig. 8); and, c) 0.2-m diameter flaw located 0.13 m deep (fig. 3).

In summary, the smaller the d/t value, the more difficult it is to detect a flaw. Additional studies [1] have shown that for a given flaw depth, t , the critical value of the flaw diameter, d , increases as the contact time of the impact increases. Thus these three variables are related.

Conclusions

This paper has focused upon the surface displacement responses produced by point impact on thick circular plates containing disk-shaped flaws. The effects on displacement waveforms and frequency spectra caused by the following test variables were determined: contact time of the impact; distance between the impact point and the response point; flaw diameter and depth; and the length of the time domain record. The following conclusions were made:

1) The contact time of the impact must be short enough so that sufficient energy is contained in the range of frequencies that will be reflected by a flaw. As the contact time increases, the range of frequencies in the input pulse decreases; therefore, the minimum flaw size that can be detected increases.

2) The point where the displacement is recorded should be kept close to the impact point to obtain maximum displacements caused by P-wave reflections.

3) The ratio of flaw diameter to flaw depth is a useful parameter for determining when planar disk-shaped flaws are likely to be detected. For a given contact time, the larger the d/t value of a flaw, the easier it is to detect the flaw.

4) Spectra obtained from time domain displacement records that are terminated before the arrival of reflections from the perimeter of the plate are much simpler to interpret, and clearly reveal the presence of flaws with smaller d/t values which would be hidden in spectra obtained from longer records.

The results of this study help to provide a theoretical basis for using the impact-echo method for finding flaws within heterogeneous solids. In addition, this paper also shows the usefulness of the finite element method as a powerful tool for solving problems of transient wave propagation in solids containing flaws.

About the authors: Mary Sansalone and Nicholas J. Carino are with the Center for Building Technology of the NBS National Engineering Laboratory.

References

- [1] Sansalone, M., and Carino, N. J., Impact-Echo: A Method for Flaw Detection in Concrete Using Transient Stress Waves, NBSIR 86-3452, September 1986, 222 pp.
- [2] Sansalone, M., Carino, N. J., and Hsu, N. N., A Finite Element Study of Transient Wave Propagation in Plates, J. Res. Natl. Bur. Stand. (U.S.) **92**, 267 (1987).
- [3] Sansalone, M., Carino, N. J., and Hsu, N. N., A Finite Element Study of the Interaction of Transient Stress Waves with Planar Flaws, J. Res. Natl. Bur. Stand. (U.S.) **92**, 279 (1987).
- [4] Sansalone, M., and Carino, N. J., Transient Impact Response of Thick Circular Plates, J. Res. Natl. Bur. Stand. (U.S.) **92**, 355 (1987).
- [5] Carino, N. J., Sansalone, M., and Hsu, N. N., A Point Source—Point Receiver Technique for Flaw Detection in Concrete, J. Amer. Concrete Inst. **83**, 199 (1986).
- [6] Sansalone, M., and Carino, N. J., Laboratory and Field Studies of the Impact-Echo Method for Flaw Detection in Concrete, to be published in Concrete International, 1987.
- [7] Carino, N. J., Sansalone, M., and Hsu, N. N., Flaw Detection in Concrete by Frequency Spectrum Analysis of Impact-Echo Waveforms, in International Advances in Nondestructive Testing, W. J. McGonagle, Ed., Gordon & Breach Science Publishers, New York, 1986.
- [8] Hallquist, J. O., A Procedure for the Solution of Finite Deformation Contact-Impact Problems by the Finite Element Method, UCRL-52066, Lawrence Livermore Laboratory, April 1976, 46 pp.
- [9] Hallquist, J. O., User's Manual for DYNA2D—An Explicit Two-Dimensional Hydrodynamic Finite Element Code with Interactive Rezoning, Lawrence Livermore Laboratory, Rev. Jan. 1984.
- [10] Proctor, Thomas M., Jr., Some Details of the NBS Conical Transducer, J. Acoustic Emission **1**, 173 (1982).
- [11] Hutchinson, J. R., Axisymmetric Flexural Vibrations of a Thick Free Circular Plate, J. Appl. Mechanics **46**, 139 (1979).
- [12] McMahan, G. W., Experimental Study of the Vibrations of Solid, Isotropic, Elastic Cylinders, J. Acoust. Soc. Amer. **36**, 85 (1964).

A Low Noise Cascode Amplifier

Volume 92

Number 6

November–December 1987

Steven R. Jefferts

Joint Institute for Laboratory
Astrophysics
University of Colorado and
National Bureau of Standards
Boulder, CO 80309

and

F. L. Walls

National Bureau of Standards
Boulder, CO 80303

We describe the design, schematics, and performance of a very low noise FET cascode input amplifier. This amplifier has noise performance of less than $1.2 \text{ nV}/\sqrt{\text{Hz}}$ and $0.25 \text{ fA}/\sqrt{\text{Hz}}$ over the 500 Hz to 50 kHz frequency range. The amplifier is presently being used in conjunction with a Penning ion trap but is applicable to a wide variety of uses requiring low noise gain in the 1 Hz to 30 MHz frequency range.

Key words: cascode amplifier; low bias current amplifier; low noise FET amplifier; noise analysis; noise current; noise voltage.

Accepted: June 8, 1987

Introduction

A low noise amplifier has been designed using a 2SK117 N channel J-FET as the input device in a cascode [1] configuration. Noise measurements on this amplifier yield a low frequency noise current of $0.25 \text{ fA}/\sqrt{\text{Hz}}$ and a voltage noise of less than $1.2 \text{ nV}/\sqrt{\text{Hz}}$ in the 500 Hz to 50 kHz region. Bloyet *et al.* [2] suggest a figure of merit of the product of the noise voltage and current as being appropriate for amplifiers of this type. This amplifier has a figure of merit of $\sim 3 \times 10^{-25} \text{ W/Hz}$, which is almost two orders of magnitude smaller than other amplifiers reported elsewhere. [2]

The amplifier described here is presently being used in conjunction with a Penning trap to detect small image currents ($\sim 0.01 \text{ pA}$) induced by ion motion in the trap. [3] This amplifier also appears to be well suited for use in noise thermometry experiments. [4]

This paper discusses some general design criteria for cascode amplifiers and draws some conclusions concerning the optimum choice of FETs for such amplifiers. A particular design having the noise performance described above is presented and analyzed. Variations of the design which either have much larger bandwidth, 30 MHz, or draw extremely low input bias current, less than 0.01 pA , are briefly discussed.

Equivalent Circuit for Noise Analysis

The schematic of the amplifier is shown in figure 1. The biasing scheme used for Q2, the common base portion of the cascode, is attractive for its simplicity and inherent low noise. However, to work properly it requires that I_{dss} [5] of Q2 be larger than I_{dss} of Q1.

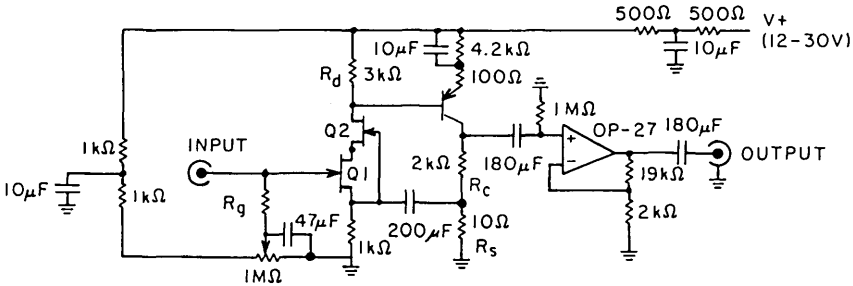


Figure 1. Schematic diagram of the low noise preamplifier. NOTE: 1) All resistors 1% metal film. 2) All capacitors are tantalum. 3) V+ must be well filtered. 4) The OP-27 power supply leads should be bypassed with 10 Ω and 0.1 μF close to the OP-AMP.

The gain of the cascode input stage is large, about 50. Hence, the noise in this stage is the dominant noise mechanism in the amplifier, and we will therefore confine our analysis to the cascode input stage and the associated biasing circuitry. The signal frequency equivalent circuit of the input stage is illustrated in figure 2. From figure 2 we can proceed to draw the noise equivalent circuit as shown in figure 3. Using this model, we can write the equivalent input noise, E_{ni} , as [6]

$$E_{ni}^2 = E_{nR_g}^2 + E_{nQ1}^2 + I_{nQ1}^2 Z_g^2 + \left(\frac{1}{K_{Q1}}\right)^2 \left[E_{nQ2}^2 + I_{nQ2}^2 R_{s1}^2 \right] + \left(\frac{1}{K_t}\right)^2 E_{nR_d}^2 \quad (1)$$

where $K_t = gm1R_d$ and $K_{Q1} = -gm1/gm2$ is the gain of the common source component of the cascode. Z_g is the impedance presented to the gate of Q1 formed by the parallel combination of C_g , the gate capacitance, and R_g , the gate bias resistor. The choice of Q2 is governed by a tradeoff between

bootstrapping C_{gd} of Q1 for lowest input capacitance and gain in Q1 suppressing voltage noise in Q2 relative to Q1. This suggests that the choice of identical FETs for Q1 and Q2 may not be optimum. For this amplifier, we chose Q2 to be a 2N4416, yielding $gm1/gm2 \sim 4$, which suppresses the voltage noise of Q2 well below that of Q1 and still provides a reduction of input capacitance from ~ 44 to ~ 11 pF.

Noise Measurements

The amplifier noise was determined by first measuring the transfer function of the amplifier on a spectrum analyzer (see fig. 4). The input capacitance was then obtained by using a known value of the capacitor in series with the input of the amplifier and measuring the change in apparent amplifier gain as a function of capacitance. In order to measure the input current noise, the gate bias resistor, R_g , was increased to $7 \times 10^{11} \Omega$ so that the term $I_{nQ1}^2 Z_g^2$ would dominate in eq (1). A measurement of the noise from 1.5 to 10 Hz coupled with the known input capacitance, C_g , allows one to write

$$\frac{1}{E_{ni}(f)} \approx \frac{1}{R_g I_{nQ1}} (1 + 2\pi C_g R_g f) \quad (2)$$

where $E_{ni}(f)$ is the equivalent noise at frequency f at the input of Q1. Using a linear regression analysis to find the slope, m , of the $1/E_{ni}$ vs f line, we can then write

$$I_{nQ1} \approx \frac{2\pi C_g}{m} \quad (3)$$

This analysis holds, assuming that the thermal noise current of R_g does not swamp the noise current of Q1 and that the perturbation of $1/f$ noise is small. The first assumption is easily checked as our

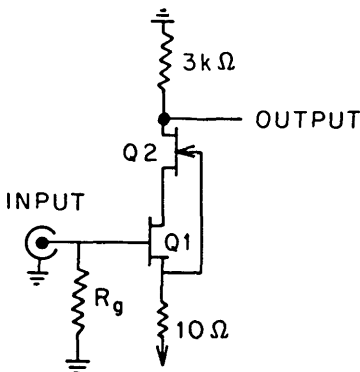


Figure 2. Signal frequency equivalent circuit of the cascode input stage.

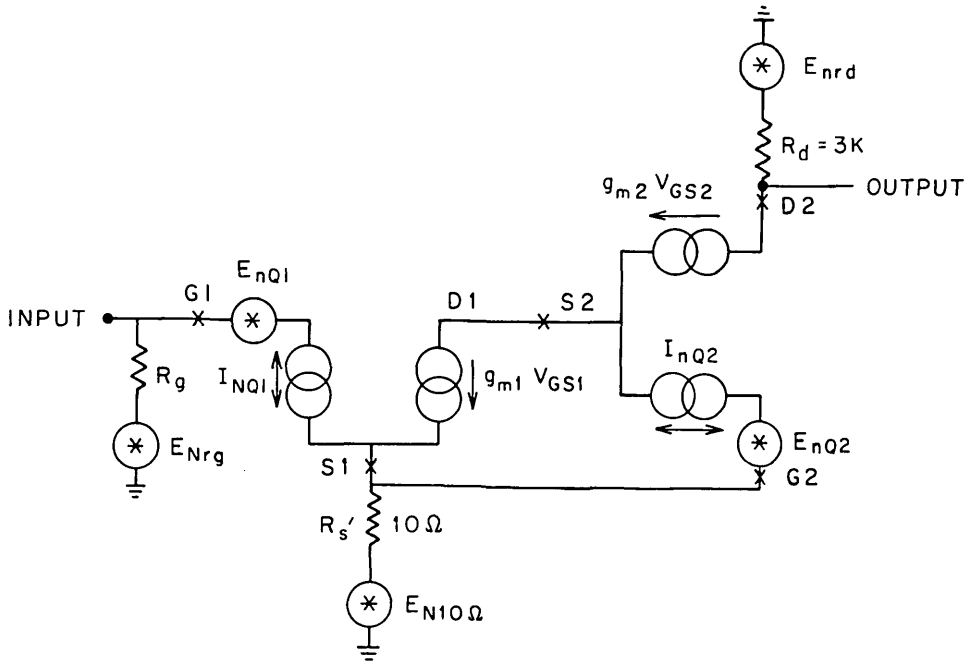


Figure 3. The noise equivalent circuit of the cascode input state.

$7 \times 10^{11} \Omega$ resistor used for R_g generates only $0.15 \text{ fA}/\sqrt{\text{Hz}}$ noise current which is of the same order of magnitude as the noise current associated with Q1. The $1/f$ contribution of current noise in both the input FET and R_g was measured to be less than $10^{-16} \text{ A}/\sqrt{\text{Hz}}$ at 1.5 Hz.

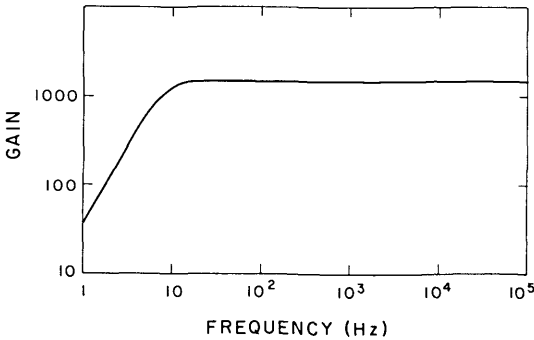


Figure 4. Measured transfer function of the amplifiers.

E_{nQ1} , the voltage noise associated with Q1, was measured by replacing the $7 \times 10^{11} \Omega$ resistor used for R_g with a 10Ω resistor. This makes the $I_{nQ1}^2 Z_g^2$ term in eq (1) insignificant and the equation can then be rewritten to yield:

$$E_{nQ1}^2 = E_{ni}^2 - E_{nRg}^2 - \left(\frac{E_{nQ2}}{K_{Q1}} \right)^2 - \left(\frac{E_{nRd}}{K_t} \right)^2 \quad (4)$$

If the noise associated with Q2, g_{m1}/g_{m2} , and the output noise are measured, one can infer the noise associated with Q1.

Results

Measurements using three different 2SK117 FETs for Q1 and a variety of different 2N4116 FETs for Q2 give the following results for the amplifier

$$E_{ni} \approx 1.1 \text{ nV}/\sqrt{\text{Hz}} \quad I_{ni} \approx 0.25 \text{ fA}/\sqrt{\text{Hz}} \quad (5)$$

Figure 5 shows the measured voltage noise as a function of frequency for the amplifier. Independent measurements with 2N4416 FETs show that the noise voltage associated with them is approximately $3 \text{ nV}/\sqrt{\text{Hz}}$. Using this value and eq (5) we can infer a noise voltage for the 2SK117 of about $0.8 \text{ nV}/\sqrt{\text{Hz}}$. It is interesting to compare this to the theoretical result derived by van der Ziel: [7]

$$e_{nQ1} = \left(\frac{2}{3} \frac{4KT}{g_{m1}} \right)^{1/2} \quad (6)$$

Using $g_{m1} = \frac{1}{60 \Omega}$, the transconductance of the

2SK117 at 3 mA drain current, we obtain $e_{nQ1} = 0.82 \text{ nV}/\sqrt{\text{Hz}}$ which is in agreement (possibly fortuitous) with the measured result.

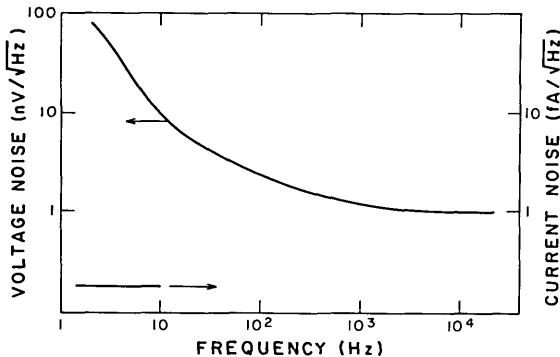


Figure 5. Measured input voltage noise.

If one measures the gate current of the input FET in a version of this amplifier in which Q2, the common gate portion of the cascode, is shorted, making the input of the amplifier a common source stage, an interesting effect occurs. The gate current, as measured by the voltage drop across R_g , decreases and finally changes sign with increasing drain current. A measurement of the noise current in this region suggests that in fact two (at least) competing currents are responsible, as the noise current is monotonically increasing in the region of apparently zero gate bias current. This is as would be expected for the noise from two competing processes. Thus, this effect is potentially useful in an application in which the amplifier must draw a minimal bias current through the gate. However, a drawback to this circuit is that the input capacitance is $\sim 50 \text{ pF}$ as opposed to $\sim 11 \text{ pF}$ for the cascode configuration. The cascode amplifier also exhibits very low input bias current, typically less than 0.3 pA for drain currents in the 3 mA range, but it does not exhibit an apparent vanishing of this bias current as does the common source configuration. It should be noted that this effect prevents us from inferring that the noise current in Q1 is due to shot noise in the measured gate current of Q1, since the true gate current is not a well determined quantity in the presence of these competing currents.

The bandwidth of the amplifier as shown in figure 1 is limited to about 500 kHz . This bandwidth limitation is, however, due to the limited bandwidth of the op-amp used for the output stage. If additional bandwidth is required, R_c and R_d should be reduced and a video amplifier should be used as the output stage.

Conclusion

We have discussed the design and test of a FET cascode input amplifier with extremely low voltage noise, less than $1.2 \text{ nV}/\sqrt{\text{Hz}}$, and extremely low current noise, $0.25 \text{ fA}/\sqrt{\text{Hz}}$.

This amplifier also has a low input capacitance of 11 pF . Thus it can be used to provide useful low noise gain from 1 Hz to more than 30 MHz . Another significant attribute is the very low bias current drawn by the amplifier, less than 0.3 pA ; a modified version of this amplifier draws even less input bias current. A short discussion of design criteria and noise mechanisms in cascode amplifiers is also provided.

Acknowledgments

The authors are grateful to John Hall and David Howe for their many useful comments and suggestions. Steven R. Jefferts would also like to thank Gordon Dunn for his support and encouragement on this project.

About the Authors: Steven R. Jefferts is with the Joint Institute for Laboratory Astrophysics University of Colorado and the National Bureau of Standards. F. L. Walls is a physicist with the Time and Frequency Division in the NBS Center for Basic Standards.

References

- [1] The term cascode amplifier refers, in a historical sense, to a pair of triode vacuum tubes operated as a grounded cathode amplification stage followed by a grounded grid amplification stage. In the case of bipolar transistors it refers to a common emitter stage followed by a common base stage and in FETs it is a common source-common gate pair as used here. Hybrid cascode amplifiers using a common source FET followed by a common base bipolar transistor are also common. See, for example, R. Q. Twiss and Y. Beers, in *Vacuum Tube Amplifiers*, MIT Radiation LABS Series edited by G. E. Valley Jr. and M. Wallman (Boston Technical Lithographers, 1963), Ch. 13.
- [2] Bloyet, D., Lepaisant, J., and Varoquaux, E., *Rev. Sci. Instrum.* **56**, 1763 (1985).
- [3] Barlow, S. E., Luine, J. A., and Dunn, G. H., *Int. J. Mass. Spectrom. Ion Proc.* **74**, 97 (1986).
- [4] Anderson, P. T., and Pipes, P. B., *Rev. Sci. Instrum.* **45**, 42 (1974).
- [5] I_{dss} is the value of the saturated drain-source current in a FET operated at zero gate source voltage.
- [6] Motchenbacher, C. D., and Fitchen, F. C., in *Low Noise Electrical Design* (Wiley, New York, 1973), p. 231.
- [7] van der Ziel, A., *Proc. IEEE* **50**, 1808 (1962).

Conferences/Events

INTERNATIONAL STANDARDS FOR NONDESTRUCTIVE TESTING

*A Report
on the Sixth Plenary
Meeting of ISO TC 135,
Yokohama, Japan,
May 11-15, 1987*

It is almost axiomatic that international standards facilitate trade. The sale of products by one country to another is certainly made easier when the buyer country knows that the goods it is purchasing conform to established standards; standards which both the buyer and seller countries may well have helped to formulate. It is for just this reason that the U.S. Department of Commerce strongly advocates the acceptance of international technical standards based on U.S. technology. The effects of international standards on testing services may not be as obvious as they are on products but they are just as significant.

Although the producer in a seller country and the user in a buyer country may both be cognizant of the international standards for a given product, there is often disagreement on the means for verifying the conformance of the product to the standards. Clearly, the producer must test the product before it leaves his plant in order to be sure that it satisfies the standards (or any other provisions that were made part of the contract). The buyer, however, may be unwilling to accept the seller's assur-

ances. He may opt to have the product retested in his own country. He may charge the costs of these tests to the manufacturer; but whether or not he does this, these costs raise the total cost of the product in the buyer country. Situations such as this make it difficult for a foreign producer to compete against a domestic producer for a share of the market in any given country, aside from any import tariffs that might be imposed by the buyer country.

In an effort to promote the sale of American products abroad, the Office of the U.S. Trade Representative has been active in international negotiations to alleviate this situation. Most of the proposals seek agreements whereby test data generated in the seller country would be accepted in the buyer country, provided that the tests were carried out in an accredited laboratory. The conditions for accreditation are still to be formulated, but it is quite clear that they will have to be contingent upon mutual agreements regarding the test methods and the qualifications of the individuals who perform the tests. In short, international standards for test methods and personnel qualifications are a prerequisite to international acceptance of test data.

For many products, tests to evaluate quality are destructive. That is, the quality of the product is evaluated, at least in part, by sampling tests of a mechanical or chemical nature which destroy the usefulness of the samples. There are numerous products, however, for which sampling and destructive testing are inappropriate and for which the quality of each and every item must be verified nondestructively. Such products are either too expensive and unique to be destroyed, or else they impact directly upon public safety. Examples include airplanes, nuclear reactors, refineries, metals processing equipment and steam generators. International agreements regarding the acceptance of test data on such products must necessarily await international standards for nondestructive test

methods and for the certification of nondestructive testing personnel.

The development of such standards is the responsibility of Technical Committee 135 on Non-Destructive Testing in the International Organization for Standardization (ISO/TC 135). (The ISO continues to use the hyphenated spelling rather than the now widely accepted version, nondestructive testing or, simply, NDT.)

The technology of NDT is generally newer than that of mechanical testing, and the development of standards for NDT, accordingly, is not as far advanced as it is for mechanical testing. Although there is a large variety of NDT methods, seven are in comparatively wide use: ultrasonics, x-ray radiography, eddy currents, magnetic particles, liquid penetrants, visual examination and leak testing. Two other methods, acoustic emission testing and neutron radiography, might be classed as "rapidly emerging."

TC 135 is organized into subcommittees (SCs) along similar lines. SC 2 on Surface Methods deals with liquid penetrant and magnetic particle testing. SC 3 on Acoustic Methods is responsible for ultrasonic and acoustic emission testing. SC 4 on Electromagnetic Methods is chiefly concerned with eddy current testing. SC 5 on Radiation Methods is responsible for x-ray, gamma ray, and neutron radiography, and SC 6 is on Leak Detection Methods. SC 7 was established only a few years ago to develop an international standard for the qualification and certification of NDT personnel for all of the methods.

At the invitation of the host country, the Sixth Plenary Meeting of ISO/TC 135 was held in Yokohama, Japan, during the week of May 11–15, 1987. Meetings of SC 2 and SC 3 were also scheduled during the same time frame, as was a meeting of Working Group 1 (WG 1) of SC 3, which is concerned with ultrasonic reference blocks.

Eight countries were represented at the meetings: The U.S.S.R., which serves as the secretariat for both TC 135 and SC 2; the U.S., which is the secretariat for SC 3; Italy, whose delegate to the meetings is the convenor for SC 3/WG 1; plus Canada, France, Federal Republic of Germany, Republic of Korea and, of course, Japan. The U.S. delegation of six members was exceeded in size only by the Japanese delegation; the Soviet delegation had four persons.

The U.S. delegation was headed by Dr. Leonard Mordfin of the National Bureau of Standards, who chairs the U.S. Technical Advisory Group for ISO/TC 135 ("the TAG"). (This Group is responsible for assessing the consensus U.S. position on

matters being developed or balloted in the Technical Committee.) Other members of the U.S. delegation included Dr. Donald G. Eitzen of NBS, who was chairman-elect of SC 3, plus four representatives from the private sector: W. E. Lawrie, the U.S. member of SC 3/WG 1; J. D. Marble, the secretary of SC 3; C. W. McKee, vice chairman of the U.S. Technical Advisory Group; and Dr. M. C. Tsao, who is the principal developer of a working document on the characterization of search units and sound fields for ultrasonic nondestructive testing. This document is based upon ASTM standards. One of the U.S. delegation's principal objectives at the meeting was to advance this document toward international acceptance. (This objective is representative of the TAG's overall goal, which is the development and promulgation of international standards for NDT which are consistent with the best practices of American industry.)

The U.S. delegation had, in fact, several objectives which it had set for itself prior to the ISO meetings. As things turned out, all of these objectives were attained. There were two occurrences, both unexpected, which may have contributed to this successful record. The first was the absence of a delegate from the United Kingdom. The U.K.'s position in recent years has run somewhat counter to the main thrust of ISO/TC 135 activities, and this has tended to cause delays and to limit progress. The second occurrence was even more surprising and it took place, or at least it began, prior to the meeting itself.

About two hours before the scheduled opening of the plenary meeting on May 11, a member of the host Japanese delegation notified Drs. Mordfin and Eitzen that the Soviet delegation wished to meet with them immediately. The Americans assented. At the meeting, the spokesman for the Soviet delegation announced that the chairman of TC 135, Professor V. V. Kljuev, had resigned from this position because "... he was no longer working in NDT" and had not come to Yokohama. Professor Kljuev is an eminent Soviet scientist with considerable expertise in NDT, so this development was quite unexpected. Even more unexpected was the Soviet spokesman's next remark, which was a request that Dr. Mordfin chair the week's meetings of TC 135. For a secretariat to appoint someone other than one of its own countrymen to chair an ISO committee meeting may well be unprecedented. To the other delegates at the meeting it was certainly unheard of. Needless to say, Dr. Mordfin accepted the invitation. Although the chair is a nonpartisan position, Dr. Mordfin's appointment unquestionably eased the U.S. delegation's attainment of its objectives at the meetings.

In retrospect, the Soviet move was a wise one. The Soviet nominee to replace Professor Kljuev as permanent chairman of TC 135 is Dr. Y. K. Fedosenko. His qualifications for the position are impeccable but his English is poor . . . and TC 135 meetings are conducted in English. Hence Dr. Fedosenko's appointment was delayed until the end of the TC 135 meetings at which time he pledged to improve his English before the next TC 135 meeting in 1989.

Aside from this, it is a matter of record that the positions of the U.S. and the U.S.S.R. in ISO TC 135 have been generally similar and quite compatible over the last few years. In fact, in matters under debate in TC 135, the U.S. finds itself allied with the Soviet Union more often than with, for example, the U.K. or France. The parallel objectives of the U.S. and the U.S.S.R. were quite evident in the Yokohama meetings. It is apparent, therefore, that the Soviet appointment of Mordfin benefited both countries.

Other notable appointments during the meeting were Mr. A. P. Degtjarev as the new permanent chairman of SC 2 on Surface Methods and Dr. Eitzen as the new permanent chairman of SC 3 on Acoustic Methods. Both men are highly acclaimed in their fields. However, Mr. Degtjarev, like Dr. Fedosenko, is new to TC 135 whereas Dr. Eitzen has been a member of the U.S. delegation to the last three plenary meetings. With this background Dr. Eitzen has, in fact, been fulfilling the chairman's responsibilities for SC 3 since September 1986, when the previous chairman resigned. Under his deft leadership in Yokohama, the subcommittee reviewed international comments which had been submitted on the U.S. working document on the characterization of ultrasonic search units and sound fields, and a resolution was adopted elevating the next revision of the document to formal ISO Draft Proposal status.

During the year prior to the Yokohama meetings, seven proposals for new work items were letter balloted through TC 135 for addition to the committee's Program of Work. All were accepted. Five of the seven proposals had been submitted by the U.S. One of these proposals was for the development of a standard for ultrasonic reference blocks; this was the basis for the establishment of Working Group 1 in SC 3. Another proposal was for a secondary calibration method for acoustic emission transducers; it is the U.S. intent that this be compatible with the acoustic emission measurement system developed at NBS. The other three new work items proposed by the U.S. deal with the standardization of neutron radiography. A team of

U.S. experts in this field is already preparing drafts for ISO consideration, based on ASTM standards. In an effort to expedite this activity, the U.S. delegation sought and obtained a resolution directing the German secretariat of SC 5 on Radiation Methods to poll its members regarding the establishment of a new working group on neutron radiography with an American convenor.

The U.S. delegation was also successful in securing a resolution relating to personnel qualification and certification. An ISO Draft Proposal on this topic is at considerable variance with American practices. Hence, the U.S. delegation sought to invite the Canadian secretariat of SC 7 on Personnel Qualification to hold its next meeting in the United States. The American Society for Nondestructive Testing, which has offered to host this meeting, feels that the two approaches to NDT personnel qualification could, perhaps, be harmonized more effectively in an American venue.

It is not at all uncommon at technical meetings for significant accomplishments to be recorded outside of the meeting rooms. This was true in Yokohama as well. Informal discussions between members of the U.S. delegation and Mr. E. Julliard of the French delegation led to a tentative agreement for the exchange of draft nondestructive testing standards which are under development in the two countries. The proposed agreement, which would involve AFNOR standards in France and ASTM and ANSI standards in the United States, is expected to facilitate the standards development process by reducing duplication of effort and by drawing the two countries into closer alignment in TC 135. Detailed procedures for implementing the agreement remain to be worked out but preliminary exchanges have already been effected. These involved French and English vocabularies for liquid penetrant testing and ultrasonic testing as a first step toward standard ISO vocabularies for these two nondestructive test methods.

Many working drafts dealing with nondestructive test methods were furthered during the week of meetings in Yokohama, most of them with significant U.S. input. It is not practical to describe this progress here in detail, but some of the drafts which were advanced in this way include documents dealing with procedures and equipment for magnetic particle testing, vocabulary for liquid penetrant inspection, ultrasonic reference blocks, ultrasonic inspection of forgings, and x-ray radiography of castings. It was also resolved that the U.S. will submit proposals for new work items to develop ISO vocabularies on magnetic particle testing and acoustic emission testing. In addition,

procedures for updating three existing ISO standards, dealing with surface methods of nondestructive testing, were reaffirmed.

Subject to approval by the German member body of ISO, the next meeting of TC 135 will be held in Berlin in 1989. Meetings that may be arranged in the meantime include SC 4 on Electromagnetic Methods in Bulgaria; SC 7 on Personnel Qualification in the United States; working group on radiography of castings in Germany; and working group on neutron radiography in Japan.

All of the delegates were uniformly complimentary about the outstanding arrangements which had been made by the Japanese hosts for these meetings. The International Conference Center in Yokohama is an exceptional facility for meetings of this kind, the banquet at the grand Hotel New Grand was exquisite, and the city of Yokohama itself proved to be thoroughly delightful.

Leonard Mordfin

U.S. Delegate to ISO/TC 135
Office of Nondestructive Evaluation
National Bureau of Standards
Gaithersburg, MD 20899

Conferences/Events

SUPERCONDUCTIVITY: CHALLENGE FOR THE FUTURE

*Federal Conference on
Commercial Applications
of Superconductivity,
Washington, DC,
July 28–29, 1987*

President Reagan outlined a new Superconductivity Initiative at the Federal Conference on Commercial Applications of Superconductivity, Washington, DC, July 28–29, 1987. The primary purpose of this conference was to stimulate commercial enterprise in high-temperature superconductor technology. Various sessions summarized the scientific facts so far as they are known, described the existing superconductor technology and attempted to draw lessons from it, speculated on the possible scope of the new technology and the problems to be solved before it can be realized, and displayed the technical resources of the Federal laboratories and the ways by which entrepreneurs might avail themselves of them. The conference received top-level political attention: it was organized by Dr. William Graham, the President's Science Advisor, and President Reagan himself gave a speech. The attendance was about 1500 people, including representatives of many Federal laboratories, universities, manufacturing companies, and a large number of consulting and market research companies.

The conference opened with a session in which Angelica Stacy (UC Berkeley), Paul Chu (Univ.

Houston) and Robert Schrieffer (UC Santa Barbara) told the now-familiar story of the processing, structure, characteristics, and theory of the new ceramic superconductors. They were followed by Sadeg Faris (Hypres) and Sibley Burnett (GA Technology), who described their experiences in bringing products of the "old" superconductor technology to market: a fast sampling oscilloscope and magnets for a magnetic resonance imaging system, respectively. They had shown in their own ways that it really can be done.

President Reagan then gave the keynote address. He started by announcing some new progress in the nuclear arms negotiations in Geneva. Then he warmed to the subject of superconductivity, with apt quotations from Benjamin Franklin and Thomas Jefferson. He concluded by outlining the Administration's Superconductivity Initiative. This includes modifications to the anti-trust laws, the patent laws, and the Freedom of Information Act, the establishment of four Superconductivity Research Centers (three at DoE laboratories and one at NBS-Boulder), and directions to various Federal scientific laboratories to increase their efforts in superconductivity. After his speech, the President toured the exhibits and the conference adjourned for lunch, at which Clayton Yeutter, the U.S. Trade Representative, gave a speech emphasizing the highly competitive nature of the potential international market and the formidable challenge from Japan.

The conference then turned to speculation about possible directions that the new superconductor technology might take. Theodore VanDuzer (UC Berkeley) gave a tutorial on the Josephson effect and other aspects of superconducting electronics. Fernand Bedard (NSA) then took up the theme of speculating about the future. He started from the notion that those who ignore history are condemned to repeat it, and reviewed the successes and failures of the past and the lessons that could

be learned from them. He saw particular promise in a hybrid superconductor/semiconductor technology: a computer might combine the advantages of superconductor logic and transmission lines with the more established technology of semiconductor cache memory, for example.

Speculation on applications to transportation and electric power were then taken up by Craig Davis (Ford) and Narain Hingorani (EPRI), respectively. The two unfinished technologies in transportation are electric cars and magnetically levitated trains. Mr. Davis showed that even high temperature superconductors could not be expected to do much for electric cars, but felt there is more promise in magnetic levitation. In electric power systems, magnetic energy storage, underground transmission, and MHD generation all deserve careful consideration. To end the first day, Roland Schmitt (GE) and Mark Rochkind (Philips) reviewed activities in high temperature superconductor research in Japan and Western Europe.

The second day opened with descriptions of two superconductor systems that are already established as medical diagnostic tools and could derive quick benefit from a high temperature superconductor technology. Sam Williamson (NYU) described remarkable achievements of magnetoencephalography, at first in medical research and more recently in diagnosis. He suggested that in the future people may want routine brain checks as part of their physical examinations. Then John Stekley (IGC) described magnetic resonance imaging, with examples of what it can now do.

After this glimpse of what is possible, John Rowell (Bell Comm) and John Hulm (Westinghouse) reminded the audience of some of the major problems that must be solved before we can realize that possibility. For all the talk of Josephson junctions, microstrip transmission lines and hybrid superconductor/semiconductor circuits, YBCO films as we know them are incompatible with microcircuit processing as we know it. They have been successful only on SrTiO₃ substrates, which are not compatible with semiconductor technology; they must be heat treated at 900°, which would destroy any nonrefractory layer in a circuit; and they are chemically very active, which will severely restrict the options for lithography. For large scale applications the present critical current density in the presence of even quite modest magnetic fields is too low by several orders of magnitude; the materials are too weak mechanically to sustain the stress from the Lorentz force; and the problem of electrodynamic stability is as yet completely unexplored. These problems are probably all soluble,

but on a time scale of years, not months.

The Federal science laboratories are clearly a great national asset in getting a commercial superconductor technology launched. Eugene McAllister (White House) and Herman Postma (ORNC) discussed all the ways in which they are accessible to private companies. The desire of the Administration is to have private industry control the development of the new commercial technology, guided by market forces, and to use the resources of the Federal laboratories to the greatest possible extent.

The formal sessions of the conference closed with an address by John Herrington, Secretary of Energy. In the afternoon there were workshop sessions for informal discussion of the topics raised at the conference. There were sessions on industrial collaboration; access to Federal laboratories; finances, venture capital and small business; advances in the science of superconductivity; and industry/university/government cooperation. With these the conference ended on the optimistic note that the present administration considers the development of a commercial superconductor technology as being a test of the ability of the U.S. free-enterprise system to compete with other nations where the government plays a more active role in commercial affairs.

Robert A. Kamper and Alan F. Clark
Electromagnetic Technology Division
National Bureau of Standards
Boulder, CO 80303

Calendar

December 3, 1987
INFORMATION RESOURCES
MANAGEMENT: STANDARDS FOR
FUTURE INFORMATION SERVICES

Location: National Bureau of Standards
Gaithersburg, MD

Increased complexity of computer systems, growing user requirements to transfer data and processes from one system to another, and strong international requirement for standards are some of the forces driving the standards development process for information technology. As a result of these forces, standards developers are producing a complex series of architectural models and standards that provide a framework for integrating data, voice, and pictures for a variety of new applications.

This conference will highlight new and emerging standards that meet user requirements for advanced integrated systems. Discussions will center on issues related to implementing these standards as part of the information resources management process. The meeting is sponsored by the National Bureau of Standards and the General Services Administration.

Contact: Shirley Radack, B151 Technology Building, National Bureau of Standards, Gaithersburg, MD 20899, 301/975-2833.

April 13-15, 1988
4th INTERNATIONAL CONFERENCE ON
METROLOGY AND PROPERTIES OF
ENGINEERING SURFACES

Location: National Bureau of Standards
Gaithersburg, MD

Metrology and properties of engineering surfaces have continued to assume great importance to both the practicing engineer and the researcher. In recent years, industry has gained increased awareness of the importance of surface preparation techniques. This international conference is the 4th in a series of meetings on the subject of metrology and properties of engineering surfaces which have

been held every 3 years since 1976. The main topics to be discussed at this meeting will be: the application of new surface techniques in industry, the development of new tactile instruments, the development of new techniques for the optical measurement of engineering surfaces, the compilation and analysis of data for specific manufacturing processes, and the relationships between surface generation and practical performance. This conference is sponsored by the National Bureau of Standards, Coventry Polytechnic, and Whitestone Business Communications.

Contact: Professor K. J. Stout, Coventry Polytechnic, Department of Manufacturing Systems, Priory Street, Coventry CV1 5FB, England, 0203 24166, ext. 278; or Dr. T. V. Vorburger, A117 Metrology Building, National Bureau of Standards, Gaithersburg, MD 20899, 301/975-3493.

April 18-22, 1988
1988 RESONANCE IONIZATION
SPECTROSCOPY CONFERENCE (RAS '88)

Location: National Bureau of Standards
Gaithersburg, MD

This meeting will bring together scientists who are studying resonance multiphoton ionization in atoms and molecules. The conference is sponsored by NBS, the Department of Energy, and the International Union of Pure and Applied Physics.

Contact: Kathy Stang, A345 Physics Building, National Bureau of Standards, Gaithersburg, MD 20899, 301/975-4513.

June 20-23, 1988
10th SYMPOSIUM ON
THERMOPHYSICAL PROPERTIES

Location: National Bureau of Standards
Gaithersburg, MD

A Call for Papers has been issued for this symposium, the 10th in a well-established series of conferences on thermophysical properties. The symposium is concerned with theoretical, experimental, and applied aspects of thermophysical properties for gases, liquids, and solids. Appropriate topics to be included in the symposium include Thermodynamic Properties, Transport Properties,

and Data Correlation. Special topics to be included in the symposium are Properties of New Materials, Properties of Gaseous and Liquid Mixtures, New Developments in Experimental Techniques, and Interpretation of Experimental Data in Terms of New Theoretical Developments. Prospective authors are requested to submit a 200–300 word abstract before December 1, 1987. The content of the abstract will be the basis for acceptance of the paper for presentation at the symposium. If the paper is accepted for presentation, then full papers should be submitted by June 23, 1988.

Contact: Dr. A. Cezairliyan, Rm. 124 Hazards Building, National Bureau of Standards, Gaithersburg, MD 20899, 301/975-5931; or Dr. J. V. Sengers, Institute for Physical Science and Technology, University of Maryland, College Park, MD 20742, 301/454-4117.

Subject and Author Index to Volume 92

A

absolute cross-section measurements.....	229
acoustic calibrations and measurements.....	129
alpha-particle counting systems.....	311
aluminum alloy.....	27
anechoic chamber measurements.....	129
anharmonicities.....	35
attenuation.....	253
Automated potentiometric system for precision measurement of the quantized Hall resistance, An.....	303

B

<i>Bright, S. J., and J. M. R. Hutchinson, The NBS large-area alpha-particle counting systems.....</i>	311
<i>Bruno, Thomas J., Catalytic cracking as the basis for a potential detector for gas chromatography.....</i>	261
<i>Burnett, Edwin D., and Victor Nedzelnisky, Free-field reciprocity calibration of microphones.....</i>	129

C

<i>Cage, Marvin E., and Giancarlo Marullo Reedt, An automated potentiometric system for precision measurement of the quantized Hall resistance.....</i>	303
calibration in QQQ instruments.....	229
calibration of far ultraviolet detector standards.....	97
calibration of microphones.....	129
calibrations of radiance temperature.....	17
candela.....	335
<i>Canfield, L. Randall, and Nils Swanson, Far ultraviolet detector standards.....</i>	97
<i>Capobianco, T. E., and J. C. Moulder, Detection and sizing of surface flaws with a SQUID-based eddy current probe.....</i>	27
<i>Carino, Nicholas J., and Mary Sansalone, Transient impact response of plates containing flaws.....</i>	369
<i>Carino, Nicholas J., and Mary Sansalone, Transient impact response of thick circular plates.....</i>	355
<i>Carino, Nicholas J., Nelson N. Hsu, and Mary Sansalone, A finite element study of the interaction of transient stress waves with planar flaws.....</i>	279
<i>Carino, Nicholas J., Nelson N. Hsu, and Mary Sansalone, A finite element study of transient wave propagation in plates.....</i>	267
cascode amplifier.....	383
catalytic cracking.....	261
Catalytic cracking as the basis for a potential detector for gas chromatography.....	261
centrifugal effects.....	35
circular plates.....	355
CODATA recommended values of the fundamental physical constants, The 1986.....	85
<i>Cohen, E. Richard, and Barry N. Taylor, The 1986 CODATA recommended values of the fundamental physical constants.....</i>	85

<i>Colclough, A. R., Two theories of experimental error.....</i>	167
concrete.....	279
consultative committee on electricity.....	55
Continuity of the meter: The redefinition of the meter and the speed of visible light, The.....	11
conversion factors.....	85
critical dimension measurement.....	187, 205
cross-section measurements in QQQ instruments.....	229
cross sections.....	229

D

<i>Davis, R. S., Note on the choice of a sensitivity weight in precision weighing.....</i>	239
dc SQUIDs for rf power measurements.....	253
Description of the thermotropic behavior of membrane bilayers in terms of Raman spectral parameters: A two-state model.....	113
Detection and sizing of surface flaws with a SQUID-based eddy current probe.....	27
detectors.....	97, 261
<i>Dheandhanoo, Seksan, and Richard I. Martinez, Instrument-independent CAD spectral databases: Absolute cross-section measurements in QQQ instruments.....</i>	229
dimensional metrology.....	205
<i>Drullinger, R. E., K. M. Evenson, C. R. Pollock, J. S. Wells, and D. A. Jennings, The continuity of the meter: The redefinition of the meter and the speed of visible light.....</i>	11

E

eddy current testing.....	27
electrical metrology.....	303
electrical units.....	55
ellipsoidal shell.....	35
error theory.....	167
<i>Evenson, K. M., C. R. Pollock, J. S. Wells, D. A. Jennings, and R. E. Drullinger, The continuity of the meter: The redefinition of the meter and the speed of visible light.....</i>	11
experimental errors.....	167

F

Far ultraviolet detector standards.....	97
finite element analysis.....	267, 279
Finite element study of the interaction of transient stress waves with planar flaws, A.....	279
Finite element study of transient wave propagation in plates, A.....	267
flaw.....	279, 369
flaw sizing.....	27
Free-field reciprocity calibration of microphones.....	129
frequency.....	11

frequency-based distributions..... 167
 frequency spectrum analysis..... 369
 fundamental physical constants 85

G

gas thermodynamic functions for water..... 35
 gas chromatography 261
 gold-point blackbody..... 17
 Green's function, stress waves with planar flaws..... 279
 Green's function, transient wave propagation
 in plates 267

H

Hamiltonian..... 35
*Hattenburg, Albert T., William R. Waters,
 and James H. Walker, The NBS scale
 of radiance temperature..... 17*
*Hsu, Nelson N., Mary Sansalone, and Nicholas J.
 Carino, A finite element study of transient wave
 propagation in plates 267*
*Hsu, Nelson N., Mary Sansalone, and Nicholas J.
 Carino, A finite element study of the interaction
 of transient stress waves with planar flaws 279*
*Hutchinson, J. M. R., and S. J. Bright, The NBS
 large-area alpha-particle counting systems..... 311*

I

Ideal gas thermodynamic functions for water..... 35
 image reconstruction 325
 imaging..... 325
 impact-echo method..... 369
 impact-echo method of stress waves with
 planar flaws..... 279
 impact-echo method of transient wave propagation
 in plates 267
 impact response of plates containing flaws 369
 impact response of thick circular plates..... 355
 Instrument-independent CAD spectral databases:
 Absolute cross-section measurements in
 QQQ instruments 229
 international..... 335
 International intercomparisons of photometric
 base units 335

J

*Jefferts, Steven R., and F. L. Walls, A low noise
 cascode amplifier 383*
*Jennings, D. A., R. E. Drullinger, K. M. Evenson,
 C. R. Pollock, and J. S. Wells, The continuity of
 the meter: The redefinition of the meter and the
 speed of visible light 11*
Josephson effect..... 55
*Joy, David C., and Michael T. Postek,
 Submicrometer microelectronics dimensional
 metrology: Scanning electron microscopy 205*

K

*Kirchhoff, William H., and Ira W. Levin, Description
 of the thermotropic behavior of membrane bilayers
 in terms of Raman spectral parameters:
 A two-state model 113*

L

large-area alpha-particle counting systems..... 311
*Larrabee, Robert D., and Diana Nyssonen,
 Submicrometer linewidth metrology in the
 optical microscope..... 187*
 laser 11
 least-squares adjustments..... 85
*Levin, Ira W., and William H. Kirchhoff, Description
 of the thermotropic behavior of membrane
 bilayers in terms of Raman spectral parameters:
 A two-state model 113*
 linewidth metrology in the optical microscope..... 187
 linewidth, scanning electron microscopes 205
 logistic function 113
 low bias current amplifier 383
 Low noise cascode amplifier 383
 low noise FET amplifier..... 383
 luminous intensity..... 335
 luminous flux..... 335

M

*Martinez, Richard I., and Seksan Dheandhanoo,
 Instrument-independent CAD spectral databases:
 Absolute cross-section measurements in QQQ
 instruments 229*
 mass metrology..... 239
 membrane 113
 meter..... 11
 metrology of microphones 129
 micrometrology 187
 microphone calibration 129
 microscopy 187
*Mielenz, Klaus D., International intercomparisons
 of photometric base units 335*
 monitoring..... 311
 Mossbauer effect..... 325
 Mossbauer imaging..... 325
 Mossbauer tomography..... 325
*Moulder, J. C., and T. E. Capobianco, Detection and
 sizing of surface flaws with a SQUID-based eddy
 current probe 27*

N

NBS large-area alpha-particle counting systems, The . 311
 NBS scale of radiance temperature, The 17
*Nedzelnitsky, Victor, and Edwin D. Burnett,
 Free-field reciprocity calibration of microphones. . 129*
 noise analysis..... 383
 noise cascode amplifier 383
 noise current..... 383
 noise voltage..... 383

nondestructive evaluation.....	27	reflection probe.....	27
nondestructive testing.....	267, 279	Report on the 17th session of the consultative committee on electricity.....	55
<i>Norton, Stephen J.</i> , Mossbauer imaging.....	325	resistance standards.....	303
Note on the choice of a sensitivity weight in precision weighing.....	239	response linearity.....	17
<i>Nyssonen, Diana, and Robert D. Larrabee</i> , Submicrometer linewidth metrology in the optical microscope.....	187	response of plates containing flaws.....	369
		response of thick circular plates.....	355
		rf measurements.....	253
O		S	
ohm.....	55, 303	<i>Sansalone, Mary, and Nicholas J. Carino</i> , Transient impact response of plates containing flaws.....	369
optical metrology.....	187	<i>Sansalone, Mary, and Nicholas J. Carino</i> , Transient impact response of thick circular plates.....	355
orthodox theory of errors.....	167	<i>Sansalone, Mary, Nicholas J. Carino, and Nelson N. Hsu</i> , A finite element study of the interaction of transient stress waves with planar flaws.....	279
		<i>Sansalone, Mary, Nicholas J. Carino, and Nelson N. Hsu</i> , A finite element study of transient wave propagation in plates.....	267
P		scale of radiance temperature.....	279
<i>Peterson, Robert L.</i> , Sinusoidal response of dc SQUIDs for rf power measurements.....	253	scanning electron microscopy.....	205
phase transition.....	113	SEM.....	205
photodiodes.....	97	semi-axes.....	35
photoionization.....	97	sensitivity weight in precision weighing.....	239
photometric base units.....	335	Sinusoidal response of dc SQUIDs for rf power measurements.....	253
photometry.....	335	sizing of surface flaws.....	27
plane-wave free-field acoustic measurements.....	129	speed of light.....	11
plate response.....	267	SQUID.....	253
plates containing flaws.....	369	standards of radiance temperature.....	17
<i>Pollock, C. R., J. S. Wells, D. A. Jennings, R. E. Drullinger, and K. M. Evenson</i> , The continuity of the meter: The redefinition of the meter and the speed of visible light.....	11	standards, methods for free-field calibration of microphones.....	129
<i>Postek, Michael T., and David C. Joy</i> , Submicrometer microelectronics dimensional metrology: Scanning electron microscopy.....	205	standards, scanning electron microscope metrology ..	205
potential detector for gas chromatography.....	261	stress wave propagation.....	267
precision weighing.....	239	stress waves with planar flaws.....	279
precision measurement of the quantized Hall resistance.....	303	subjectivist distributions.....	167
process-control metrology.....	187	Submicrometer linewidth metrology in the optical microscope.....	187
proportional counting.....	311	Submicrometer microelectronics dimensional metrology: Scanning electron microscopy.....	205
		substitution weighing.....	239
Q		superconducting quantum interference device.....	27
quantized Hall resistance.....	303	superconductivity.....	253
quantum efficiency.....	97	surface flaws with a SQUID-based eddy current probe.....	27
quantum Hall effect.....	55	<i>Swanson, Nils, and L. Randall Canfield</i> , Far ultraviolet detector standards.....	97
		systematic errors.....	167
R		T	
radiance temperature.....	17	tandem mass spectrometry.....	229
radioactivity.....	311	target thickness.....	229
Raman spectroscopy.....	113	task group on fundamental constants.....	85
random errors.....	167	<i>Taylor, B. N.</i> , Report on the 17th session of the consultative committee on electricity.....	55
randomistic theory of errors.....	167	<i>Taylor, Barry N., and E. Richard Cohen</i> , The 1986 CODATA recommended values of the fundamental physical constants.....	85
reciprocity calibration methods.....	129	thermotropic behavior of membrane bilayers in terms of Raman spectral parameters.....	113
recommended values.....	85		
redefinition of the meter and the speed of visible light.....	11		
<i>Reedix, Giancarlo Marullo, and Marvin E. Cage</i> , An automated potentiometric system for precision measurement of the quantized Hall resistance.....	303		

tomographic image reconstruction	325
traceability	129
transducer calibration (reciprocity)	129
Transient impact response of plates containing flaws .	369
Transient impact response of thick circular plates	355
transient wave propagation in plates	267
transposition weighing	239
tungsten-strip lamps	17
Two theories of experimental error	167
two-state model	113

U

ultraviolet detector standards	17
--------------------------------------	----

V

values of the fundamental physical constants	85
vibrational states	35
volt	55

W, X, Y, Z

<i>Walker, James H., Albert T. Hattenburg, and William R. Waters, The NBS scale of radiance temperature</i>	17
<i>Walls, F. L., and Steven R. Jefferts, A low noise cascode amplifier</i>	383
<i>Waters, William R., James H. Walker, and Albert T. Hattenburg, The NBS scale of radiance temperature</i>	17
wave propagation	279
weighing	239
<i>Wells, J. S., D. A. Jennings, R. E. Drullinger, K. M. Evenson, and C. R. Pollock, The continuity of the meter: The redefinition of the meter and the speed of visible light</i>	11
<i>Woolley, Harold W., Ideal gas thermodynamic functions for water</i>	35